ASTRONOMY & ASTROPHYSICS
SUPPLEMENT SERIES

Astron. Astrophys. Suppl. Ser. **131**, 153–166 (1998)

Atomic data from the IRON project

XXXI. Electron impact excitation of optically allowed and intercombination electric dipole transitions in Fe XII⋆

A.M. Binello[1], **H.E. Mason**[1], **and P.J. Storey**[2]

[1] Department of Applied Mathematics and Theoretical Physics, University of Cambridge, Silver Street, Cambridge CB3 9EW, UK
[2] Department of Physics and Astronomy, University College London, Gower Street, London WC1 E6BT, UK

Received January 9; accepted February 24, 1998

Abstract. A new, accurate set of electron impact collisional data is presented, relating to all electric dipole fine-structure transitions between the ground $3s^2\,3p^3$ and the first two excited $3s\,3p^4$, $3s^2\,3p^2\,3d$ configurations in Fe XII (Fe^{11+}). Theoretical energies have been obtained with a multi-configuration atomic structure calculation. The *R-matrix* method, coupled with the *Coulomb-Bethe* (CBe) approximation for the high partial wave contributions to the collision strengths, has been employed in the $Fe^{11+} - e^-$ scattering problem. The data presented in this paper form part of the *IRON Project* effort to provide the most accurate atomic data available to date for all the iron ions (Hummer et al. 1993).

Key words: ion — atomic data — atomic processes — Sun: UV radiation

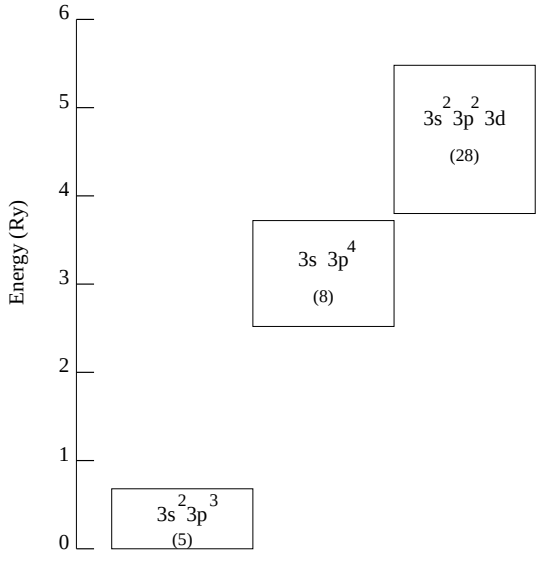

Fig. 1. Energy distribution of the three lowest configurations in Fe XII. Numbers in parenthesis indicate the number of levels in that configuration

1. Introduction

Bright resonance lines due to strong electric dipole transitions in Fe XII have been identified in solar spectra since the early days of UV rocket and space observations. The sensitivity to electron density of line ratios involving these resonance lines (Kastner & Mason 1978; Withbroe & Raymond 1984) has proved to be a powerful diagnostic technique for investigating the physical conditions in the solar corona. The Fe XII ion is expected to attain peak abundance at $\log T_e = 6.15$ in conditions of ionisation equilibrium (Arnauld & Raymond 1992). The most recent *Solar Heliospheric Observatory* (SOHO) observations have provided a wealth of fascinating images and spectral data in the strongest Fe XII optically allowed lines such as at 195 Å (EIT – *Extreme ultraviolet Imaging Telescope*) and at 364.5 Å (CDS – *Coronal Diagnostic Spectrometer*, Mason et al. 1997). Electric dipole transitions also play a key role in determining the relative populations of the excited levels of the ground configuration through collisional excitation and radiative cascade. This occurs because their excitation rates are considerably greater than the corresponding quantities relative to the forbidden transitions. The ratios of forbidden lines within the ground configuration of Fe XII are important for diagnostic purposes (Feldman et al. 1983).

Send offprint requests to: A. Binello

⋆ Tables 1 to 9 are also available in electronic form at the CDS via ftp to cdsarc.u-strasbg.fr (130.79.128.5) or via http://cdsweb.u-strasbg.fr/Abstract.html

Table 1. Energy levels (cm^{-1}) for the lowest three configurations in Fe XII. For values in *italic* see text

Configuration	Level	E_{obs}	E_{th}
$3s^2\,3p^3$	$^4S^o_{3/2}$	0	0
	$^2D^o_{3/2}$	41555	44477
	$^2D^o_{5/2}$	46088	49049
	$^2P^o_{1/2}$	74108	77755
	$^2P^o_{3/2}$	80515	84059
$3s\,3p^4$	$^4P_{5/2}$	274373	274093
	$^4P_{3/2}$	284005	283799
	$^4P_{1/2}$	288307	288194
	$^2D_{3/2}$	339761	343277
	$^2D_{5/2}$	341703	345171
	$^2P_{3/2}$	389668	396678
	$^2P_{1/2}$	394352	401278
	$^2S_{1/2}$	410401	417216
$3s^2\,3p^2\,3d$	$(^3P)\,^4F_{3/2}$	*420258*	435809
	$(^3P)\,^4F_{5/2}$	*424022*	439573
	$(^3P)\,^4F_{7/2}$	*429530*	445081
	$(^3P)\,^4F_{9/2}$	*436385*	451936
	$(^1D)\,^2F_{5/2}$	*437194*	452611
	$(^3P)\,^4D_{1/2}$	*440316*	455867
	$(^3P)\,^4D_{7/2}$	*440941*	456492
	$(^3P)\,^4D_{3/2}$	*441414*	456966
	$(^3P)\,^4D_{5/2}$	*446055*	461606
	$(^1D)\,^2F_{7/2}$	*455887*	471304
	$(^1D)\,^2G_{7/2}$	*491903*	507320
	$(^1D)\,^2G_{9/2}$	*494879*	510296
	$(^3P)\,^2P_{3/2}$	501800	513685
	$(^3P)\,^4P_{5/2}$	512510	524880
	$(^3P)\,^2P_{1/2}$	513850	525739
	$(^3P)\,^4P_{3/2}$	516740	528938
	$(^3P)\,^4P_{1/2}$	519770	531540
	$(^1S)\,^2D_{3/2}$	526120	539623
	$(^1S)\,^2D_{5/2}$	538040	550427
	$(^1D)\,^2D_{3/2}$	554030	567870
	$(^1D)\,^2D_{5/2}$	554610	569025
	$(^1D)\,^2P_{1/2}$	568940	587307
	$(^3P)\,^2F_{5/2}$	576740	593418
	$(^1D)\,^2P_{3/2}$	577740	595306
	$(^1D)\,^2S_{1/2}$	579630	593956
	$(^3P)\,^2F_{7/2}$	581180	597798
	$(^3P)\,^2D_{5/2}$	603930	621026
	$(^3P)\,^2D_{3/2}$	605480	622632

Past calculations of Fe XII electric dipole atomic data include those of Flower (1977) (henceforward referred to as F77), Bromage et al. (1978); Fawcett (1986) and Tayal & Henry (1986), as far as structure and radiative data is concerned. Electron collisional data have been published by F77 and Tayal & Henry (1988) (henceforward referred to as TH88). In a previous paper in the *IRON Project* series[1] (Binello et al. 1998, henceforward referred to as BMS) we presented atomic data for the forbidden transitions within the ground configuration of Fe XII and discussed the limitations of a previous corresponding calculation by Tayal et al. (1987). In this paper we want to complement those results by presenting new electron scattering data for electric dipole fine-structure transitions between the ground $3s^2\,3p^3$ and the first two excited $3s\,3p^4$, $3s^2\,3p^2\,3d$ configurations in Fe XII. A schematic diagram of the relative position in energy of these three configurations is shown in Fig. 1. As the techniques employed in the atomic structure and electron scattering problems, and the computer codes used, have already been described in BMS, in the following sections we will discuss only the details related to the particular type of transitions considered here. In Sect. 2 an account of the electron scattering computation and related results will be given. A detailed comparison with previous results will be the subject of Sect. 3. Finally, discussion and conclusions will be presented in Sect. 4.

[1] A complete list of *IRON Project* publications and papers in press can be found at http://www.am.qub.ac.uk

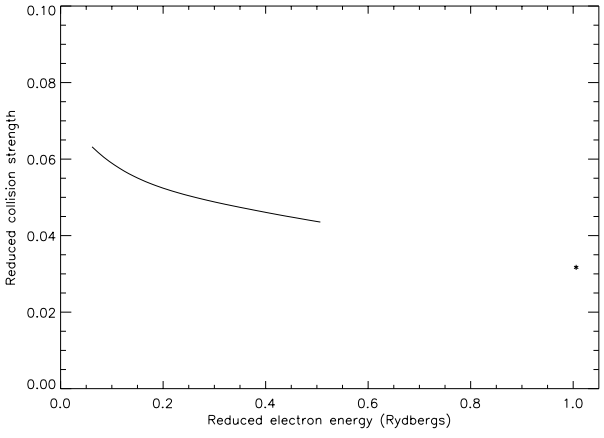

Fig. 2. Reduced collision strength vs. reduced energy for the $3s^2\,3p^3\,^2P^o_{1/2} \rightarrow 3s\,3p^4\,^2S_{1/2}$ optically allowed transition. The asterisk shows the high energy Bethe limit

2. The $Fe^{11+} - e^-$ scattering problem

2.1. 19 term R-matrix *computation*

The *R-matrix* technique, implemented in the Queen's University Belfast *R-matrix* suite of programs (Berrington et al. 1995), has been used for the computation of the low partial wave contributions to the total collision strengths $\Omega\,(i \rightarrow j) = \sum_l \Omega_l\,(i \rightarrow j)$, $\Omega_l\,(i \rightarrow j)$ being the partial collision strength for transition $i \rightarrow j$, with l the orbital angular momentum of the scattered electron. For the calculation of collision strengths for electric dipole transitions within the *R-matrix* approach we included contributions coming from partial waves as high as $l_{max} = 16$, such that

$$\Omega^{R-m} = \sum_{l=0}^{16} \Omega_l^{R-m}. \quad (1)$$

This will be shown to be a proper choice in order to ensure convergence between the low l *R-matrix* results and the high l *Coulomb-Bethe* (CBe) ones (see

Table 2. Intermediate states ($S\,L\,\pi$) included in the expansion of the $(N+1)-$e collision complex wavefunction

	even parity		odd parity	
	$(2S_{N+1}+1) = 1, 3$	$(2S_{N+1}+1) = 5$	$(2S_{N+1}+1) = 1, 3$	$(2S_{N+1}+1) = 5$
L_{N+1}	$0 \rightarrow 20$	$0 \rightarrow 19$	$0 \rightarrow 19$	$0 \rightarrow 18$

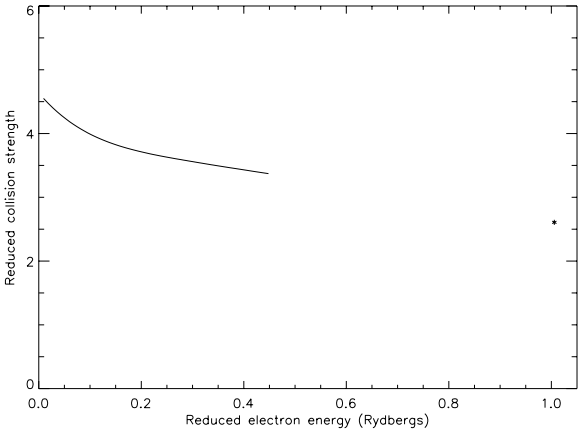

Fig. 3. Reduced collision strength vs. reduced energy for the $3s^2\,3p^3\,{}^2P^o_{3/2} \rightarrow 3s^2\,3p^2\,3d\,({}^3P)\,{}^2D_{5/2}$ optically allowed transition. The asterisk shows the high energy Bethe limit

Sect. 2.2). The expansion of the total wavefunction for the Fe^{11+} target included the lowest 19 LS coupling terms $3s^2\,3p^3\ {}^4S^o,\ {}^2D^o,\ {}^2P^o,\ 3s\,3p^4\ {}^4P,\ {}^2D,\ {}^2P,\ {}^2S,\ 3s^2\,3p^2\,3d\ ({}^3P)\,{}^4F,\ ({}^3P)\,{}^4D,\ ({}^1D)\,{}^2F,\ ({}^1D)\,{}^2G,\ ({}^3P)\,{}^2P,\ ({}^3P)\,{}^4P,\ ({}^1S)\,{}^2D\ ({}^1D)\,{}^2D,\ ({}^1D)\,{}^2S,\ ({}^1D)\,{}^2P,\ ({}^3P)\,{}^2F,\ ({}^3P)\,{}^2D$. In Table 1 we list all the fine-structure levels belonging to the $3s^2\,3p^3$, $3s\,3p^4$, $3s^2\,3p^2\,3d$ configurations along with the relative observed energy values, taken from Corliss & Sugar (1982) and Jupen et al. (1993). Italic type in the column listing the observed energies indicates that experimental values are not yet available for those levels. In these cases theoretical energies computed with the atomic structure program SUPERSTRUCTURE (Eissner et al. 1974; Nussbaumer & Storey 1978) were empirically corrected with the procedure described in BMS. The theoretical energies listed in Table 1 have been obtained with a 24 configuration atomic model including those configurations with one electron in 4s, 4p, 4d and 4f orbitals of spectroscopic type (set 3 in BMS). The energies for the 19 target LS coupling terms listed above were obtained as weighted averages over the fine-structure observed energies given in Table 1 and were listed in Table 5 of BMS. The 19 target terms were represented by configuration interaction (CI) expansions constructed with a common set of radial waves, describing the radial charge distribution of the 1s, 2s, 2p, 3s, 3p and 3d bound electrons. These radial functions were obtained with SUPERSTRUCTURE adopting the 12 configuration basis described in BMS. A total of 16 continuum orbitals was included in the calculation and the *R-matrix* "box" boundary was set at 3.09 a.u. For the expansion of the $(N+1)-$e collision complex wavefunction we combined in all possible fashions one scattering electron having spin $s = 1/2$ and $l = 0, \ldots, 16$ with the LS coupling target terms listed above. In such a way we obtained a total of 121 intermediate states specified in Table 2. The calculation was performed with a very fine energy mesh of $1.59375\ 10^{-3}$ Ry in the closed channel region (2.55 to 5.5 Ry), in order to delineate the resonance structure of the collision strength below the highest excitation threshold. In the open channel region (5.5 to 100 Ry), on the contrary, a much coarser energy mesh was chosen, namely 0.5 Ry between 5.5 Ry and 20 Ry, 1 Ry between 20 Ry and 50 Ry, and 5 Ry between 50 Ry and 100 Ry. This proved to be sufficient to describe the variation of the collision strengths as a function of energy.

2.2. Top-up in l

A top-up procedure to account for the missing partial wave contributions to Ω coming from $l > 16$ was necessary in the open channel region in order to provide final reliable results. The application of geometric series properties to the partial collision strengths, discussed in BMS, proved to be inappropriate to the case of strong electric dipole transitions. For these transitions we estimated the contributions from partial waves with $l = 17 \rightarrow \infty$ with the *Coulomb-Bethe* (CBe) approximation (van Regemorter 1960; Burgess et al. 1970). The CBe method implies the "long range" approximation, where only the long range potential of the target is effective in the interaction with the scattering electron. As stated in van Regemorter (1960) the "long range" approximation is only valid for sufficiently high values of l, i.e. "distant" encounters between the target and the colliding electron. Burgess & Tully (1978) define "distant" as those partial waves with

$$l \geq \left(k^2\,r_0^2\ +\ 2\,z\,r_0\right)^{1/2}\ -\ \frac{1}{2} \qquad (2)$$

where z is the ion net charge, r_0 the radius of the spherical region containing the target charge distribution and k^2 the scattering electron energy in Ry. This formula gives a convenient criterion to estimate the lowest "safe" partial wave contribution to the total collision strength which can be computed with the CBe technique, given a specific target model and an energy range where collision strengths are required. Our choice of $l > 16$ for the CBe partial wave contributions satisfied Eq. (2) and the convergence of *R-matrix* and *Coulomb-Bethe* results for the strongest electric dipole transitions is shown in Table 3. The convergence of the two methods at $E = 100$ Ry, for $l = 16$,

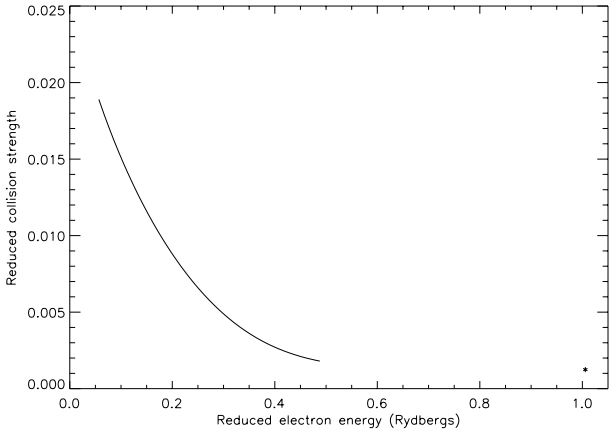

Fig. 4. Reduced collision strength vs. reduced energy for the $3s^2\,3p^3\,{}^4S^o_{3/2} \rightarrow 3s\,3p^4\,{}^2P_{1/2}$ intercombination transition. The asterisk shows the high energy Bethe limit

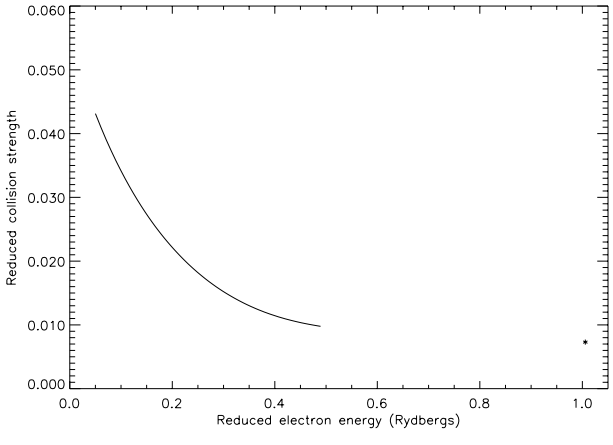

Fig. 5. Reduced collision strength vs. reduced energy for the $3s^2\,3p^3\,{}^2D^o_{3/2} \rightarrow 3s^2\,3p^2\,3d\,({}^3P)\,{}^4F_{3/2}$ intercombination transition. The asterisk shows the high energy Bethe limit

is in all cases better than 1%. After topping-up the *R-matrix* collision strengths with the CBe contributions for $l > 16$, great care has been taken in checking the correct convergence to the high energy Bethe limits of the topped-up reduced collision strengths, Ω_r, as a function of reduced energy, E_r, as defined by Burgess & Tully (1992). Figures 2 to 5 show a few examples of plots of Ω_r vs. E_r, in the open channel energy region, for selected electric dipole transitions.

2.3. Top-up in energy

The assumption of constant Ω at $E > 100\,\mathrm{Ry}$ in integrating the collision strengths over a Maxwellian distribution of electron energies, well justified in BMS for the forbidden transitions, is not appropriate to the strong electric dipole transitions we are treating here. In fact Burgess & Tully (1992) classify these transitions as type 1 and give a high energy limiting behaviour of the kind

$$\Omega \sim \mathrm{const} \cdot \ln(E) \qquad (3)$$

deduced from the *Bethe* approximation. By using the scaling rules in Eqs. (5) and (6) of Burgess & Tully (1992) and Eq. (7) of Burgess & Tully (1978), it can be shown that, in the limit of high E, Ω_r is a linear function of E_r. We therefore scaled our collision strengths as suggested in Burgess & Tully (1992) for type 1 transitions and performed linear interpolation of Ω_r between $\Omega_r\,(100\,\mathrm{Ry})$ and $\Omega_r\,(\infty)$, given by the Bethe limit $4\,\omega_i\,f_{ij}/E_{ij}$, where ω_i is the statistical weight of the initial level, f_{ij} the oscillator strength and E_{ij} the excitation energy of the transition $i \rightarrow j$. By applying the inverse transformation to these interpolated values we obtained a set of Ω values between 100 Ry and 9900 Ry, with an energy mesh of 100 Ry, which takes proper account of the logarithmic increase of Ω with E. The integration of the extended set of collision strengths is discussed in the following section.

2.4. Results

Topped-up final collision strengths $\Omega\,(i \rightarrow j)$ for all electric dipole fine-structure transitions between the ground $3s^2\,3p^3$ and the first excited $3s\,3p^4$ configurations are compared with previous calculations in Table 4 at two energy values in the open channel region. Table 5 shows a similar comparison for all electric dipole transitions between the ground $3s^2\,3p^3$ and the second excited $3s^2\,3p^2\,3d$ configurations. The complete set of collision strength values at all electron energies considered in our scattering calculation (see Sect. 2.1), in the closed as well as open channel energy region, can be obtained in electronic format via anonymous ftp from the *IRON Project* data bank at iron.am.qub.ac.uk. *Effective*, or *thermally averaged* collision strengths, given by

$$\Upsilon\,(i \rightarrow j) = \int_0^\infty \Omega\,(i \rightarrow j) \exp\left(-\frac{E_j}{kT_e}\right) \mathrm{d}\left(\frac{E_j}{kT_e}\right) \qquad (4)$$

where E_j is the colliding electron kinetic energy after excitation, have been obtained by integrating the collision strengths using the linear interpolation technique described in Burgess & Tully (1992). The extended set of original plus interpolated $\Omega\,(i \rightarrow j)$ values was used in the integration process and it was assumed $\Omega\,(9900\,\mathrm{Ry} < E < \infty) = \Omega\,(9900\,\mathrm{Ry})$. The exponential factor in Eq. (4) drops off rapidly with increasing energy so that the contribution to $\Upsilon\,(i \rightarrow j)$ coming from the energy region $E_{\min} < E < \infty$, where Ω is taken constant, decreases rapidly with increasing $E_{\min}$. For example, for $T_e = 10^7$ K, this contribution was as high as 25% for $E_{\min} = 100\,\mathrm{Ry}$, for most electric dipole transitions we studied, dropping down to a typical 10^{-65}% (!) when the extended set of Ω's is integrated ($E_{\min} = 9900\,\mathrm{Ry}$). Effective collision strengths for

Table 3. Partial *R-matrix* (*Rm*) and *Coulomb-Bethe* (*CBe*) collision strengths Ω_l for $l = 14$, 15, 16 at $E = 100$ Ry

Transition	$l = 14$		$l = 15$		$l = 16$	
	$\Omega_l^{\rm Rm}$	$\Omega_l^{\rm CBe}$	$\Omega_l^{\rm Rm}$	$\Omega_l^{\rm CBe}$	$\Omega_l^{\rm Rm}$	$\Omega_l^{\rm CBe}$
$3s^2\,3p^3\,{}^4S^o_{3/2} - 3s^2\,3p^2\,3d\,({}^3P)\,{}^4P_{5/2}$	0.38716	0.39590	0.36047	0.36560	0.33675	0.33866
$3s^2\,3p^3\,{}^4S^o_{3/2} - 3s^2\,3p^2\,3d\,({}^3P)\,{}^4P_{3/2}$	0.25832	0.26422	0.24053	0.24400	0.22473	0.22602
$3s^2\,3p^3\,{}^2D^o_{3/2} - 3s^2\,3p^2\,3d\,({}^1D)\,{}^2D_{3/2}$	0.17466	0.17877	0.16261	0.16513	0.15166	0.15301
$3s^2\,3p^3\,{}^2D^o_{3/2} - 3s^2\,3p^2\,3d\,({}^3P)\,{}^2F_{5/2}$	0.39483	0.40446	0.36736	0.37307	0.34285	0.34516
$3s^2\,3p^3\,{}^2D^o_{5/2} - 3s\,3p^4\,{}^2D_{5/2}$	0.06577	0.06681	0.06168	0.06232	0.05827	0.05836
$3s^2\,3p^3\,{}^2D^o_{5/2} - 3s\,3p^4\,{}^2P_{3/2}$	0.07828	0.07945	0.07330	0.07398	0.06882	0.06913
$3s^2\,3p^3\,{}^2D^o_{5/2} - 3s^2\,3p^2\,3d\,({}^3P)\,{}^2P_{3/2}$	0.19621	0.19947	0.18303	0.18475	0.17080	0.17167
$3s^2\,3p^3\,{}^2D^o_{5/2} - 3s^2\,3p^2\,3d\,({}^1D)\,{}^2D_{5/2}$	0.20486	0.20813	0.19060	0.19226	0.17793	0.17815
$3s^2\,3p^3\,{}^2D^o_{5/2} - 3s^2\,3p^2\,3d\,({}^3P)\,{}^2F_{7/2}$	0.55998	0.57367	0.52110	0.52914	0.48617	0.48956
$3s^2\,3p^3\,{}^2P^o_{1/2} - 3s^2\,3p^2\,3d\,({}^1D)\,{}^2S_{1/2}$	0.10689	0.10982	0.09960	0.10153	0.09322	0.09416
$3s^2\,3p^3\,{}^2P^o_{1/2} - 3s^2\,3p^2\,3d\,({}^3P)\,{}^2D_{3/2}$	0.18992	0.19515	0.17675	0.18010	0.16508	0.16672
$3s^2\,3p^3\,{}^2P^o_{3/2} - 3s^2\,3p^2\,3d\,({}^1D)\,{}^2P_{3/2}$	0.16892	0.17266	0.15741	0.15961	0.14747	0.14802
$3s^2\,3p^3\,{}^2P^o_{3/2} - 3s^2\,3p^2\,3d\,({}^3P)\,{}^2D_{5/2}$	0.38133	0.38938	0.35488	0.35935	0.33116	0.33265

all electric dipole $3s^2\,3p^3 \rightarrow 3s\,3p^4$ fine-structure transitions are given in Tables 6 and 7 for two different temperature ranges. Similar data are presented in Tables 8 and 9 for all electric dipole $3s^2\,3p^3 \rightarrow 3s^2\,3p^2\,3d$ fine-structure transitions.

3. Comparison with previous calculations

3.1. $3s^2\,3p^3 - 3s\,3p^4$ transitions

Previous calculations of collision strengths for the $3s^2\,3p^3 \rightarrow 3s\,3p^4$ electric dipole transitions in Fe XII by F77 and TH88 are available for a detailed comparison with the present results.

F77 adopted a *distorted wave* approach coupled with a limited target model including 4 configurations ($3s^2\,3p^3$, $3s\,3p^4$, $3s^2\,3p^2\,3d$ and $3p^5$), and computed collision strengths at only one value of energy (6.6 Ry). Due to the approximation used in the scattering process and to limitations in computational resources, resonance effects and the variation of Ω with E could not be explored. In Table 4 we compare the two sets of data by choosing a cut-off of $\pm\,50\%$ of the present results. Values in F77 which do not agree within 50% with our collision strengths have been denoted with the superscript ^{a}. Out of 35 transitions, 6 (17%) do not satisfy the $\pm\,50\%$ criterion and have not been included in the analysis. It should be noted that of these 6 transitions only 1 has $\Omega > 0.1$ in our calculation. For the remaining 29 transitions we find an average difference of 15% from our results.

TH88 adopted a more comprehensive target representation, also including correlation orbitals, and used the more sophisticated *R-matrix* approach in their scattering calculation. Details of their computation have been extensively discussed in relation to ours in BMS. We compare the two sets of collision strengths in Table 4 at the lowest (6.6 Ry) and highest (30 Ry) energies for which they tabulate values. At 6.6 Ry 10 transitions (29%) do not satisfy the $\pm\,50\%$ criterion and we find an average difference of 18% from our data for the remaining values. It is important to note that all the Ω's excluded are < 0.1 in our computation. At 30 Ry we find an average difference of 16% from our data, after exclusion of 9 transitions (26%), of which only 1 has $\Omega > 0.1$ in our set. A comparison over the entire energy range tabulated by TH88 reveals that the two sets of Ω's have the same trend as a function of E.

We stress the point that all the collision strength values which show the most severe disagreement between the different sets of calculations, up to more than an order of magnitude in some cases, are "weak" transitions, i.e. transitions with $\Omega \leq 0.1$. For these transitions the strong mixing of levels and consequent cancellation effects in the matrix elements, which depend on the particular choice of the target model, are more likely to introduce big discrepancies in the collision strengths, as shown by the above analysis. This shows once more the importance of a proper choice of target representation in a scattering calculation, i.e. one in which full account is taken of interaction effects between configurations of a parity complex.

As is the case for the forbidden transitions within the $3s^2\,3p^3$ ground configuration (Tayal et al. 1987), a large discontinuity between the Ω values at 4 Ry and at 6.6 Ry is evident in TH88 electric dipole collision strengths. As discussed in BMS, this is likely to be due to residual pseudo-resonance effects in the open channel energy region and, because of this, it should not be surprising that our collision strengths at 6.6 Ry agree marginally better with F77, despite the more sophisticated approach adopted in the present work and by TH88.

The problems introduced by these non-physical pseudo-resonances in the open channel energy region and by the extra resonances below the highest

Table 4. Collision strengths for all electric dipole fine-structure transitions between the ground $3s^2\,3p^3$ and the first excited $3s\,3p^4$ configurations in Fe XII. [a] see text

Transition ($3s^2\,3p^3 \rightarrow 3s\,3p^4$)	E (Ry)				
	6.6			30	
	present work	Tayal & Henry (1988)	Flower (1977)	present work	Tayal & Henry (1988)
$^4S^o_{3/2} - {}^4P_{5/2}$	0.942	0.700	1.110	1.267	1.160
$^4S^o_{3/2} - {}^4P_{3/2}$	0.610	0.490	0.760	0.822	0.780
$^4S^o_{3/2} - {}^4P_{1/2}$	0.306	0.260	0.390	0.413	0.400
$^4S^o_{3/2} - {}^2D_{3/2}$	0.004	0.007[a]	0.003	0.002	0.007[a]
$^4S^o_{3/2} - {}^2D_{5/2}$	0.002	0.030[a]	0.005[a]	0.003	0.041[a]
$^4S^o_{3/2} - {}^2P_{3/2}$	0.068	0.074	0.066	0.028	0.028
$^4S^o_{3/2} - {}^2P_{1/2}$	0.023	0.019	0.025	0.011	0.006
$^4S^o_{3/2} - {}^2S_{1/2}$	0.012	0.028[a]	0.013	0.008	0.016[a]
$^2D^o_{3/2} - {}^4P_{5/2}$	0.034	0.035	0.036	0.024	0.013
$^2D^o_{3/2} - {}^4P_{3/2}$	0.021	0.028	0.017	0.007	0.013[a]
$^2D^o_{3/2} - {}^4P_{1/2}$	0.010	0.013	0.008	0.005	0.003
$^2D^o_{3/2} - {}^2D_{3/2}$	0.957	0.820	1.030	1.346	1.280
$^2D^o_{3/2} - {}^2D_{5/2}$	0.059	0.085	0.068	0.037	0.040
$^2D^o_{3/2} - {}^2P_{3/2}$	0.172	0.200	0.130	0.238	0.290
$^2D^o_{3/2} - {}^2P_{1/2}$	0.566	0.460	0.650	0.821	0.660
$^2D^o_{3/2} - {}^2S_{1/2}$	0.037	0.110[a]	0.030	0.047	0.150[a]
$^2D^o_{5/2} - {}^4P_{5/2}$	0.063	0.072	0.055	0.046	0.042
$^2D^o_{5/2} - {}^4P_{3/2}$	0.017	0.023	0.014	0.008	0.009
$^2D^o_{5/2} - {}^2D_{3/2}$	0.070	0.098	0.076	0.041	0.055
$^2D^o_{5/2} - {}^2D_{5/2}$	1.278	1.130	1.480	1.748	1.760
$^2D^o_{5/2} - {}^2P_{3/2}$	1.336	1.270	1.370	1.911	1.830
$^2P^o_{1/2} - {}^4P_{3/2}$	0.014	0.025[a]	0.013	0.005	0.007
$^2P^o_{1/2} - {}^4P_{1/2}$	0.015	0.014	0.014	0.010	0.004[a]
$^2P^o_{1/2} - {}^2D_{3/2}$	0.129	0.130	0.069	0.171	0.200
$^2P^o_{1/2} - {}^2P_{3/2}$	0.094	0.100	0.043[a]	0.122	0.130
$^2P^o_{1/2} - {}^2P_{1/2}$	0.388	0.410	0.330	0.554	0.620
$^2P^o_{1/2} - {}^2S_{1/2}$	0.080	0.030[a]	0.150[a]	0.116	0.035[a]
$^2P^o_{3/2} - {}^4P_{5/2}$	0.026	0.090[a]	0.026	0.013	0.079[a]
$^2P^o_{3/2} - {}^4P_{3/2}$	0.032	0.050[a]	0.034	0.022	0.032
$^2P^o_{3/2} - {}^4P_{1/2}$	0.013	0.020[a]	0.012	0.005	0.005
$^2P^o_{3/2} - {}^2D_{3/2}$	0.040	0.054	0.081[a]	0.026	0.021
$^2P^o_{3/2} - {}^2D_{5/2}$	0.403	0.340	0.260	0.538	0.540
$^2P^o_{3/2} - {}^2P_{3/2}$	0.177	0.210	0.058[a]	0.237	0.280
$^2P^o_{3/2} - {}^2P_{1/2}$	0.010	0.038[a]	0.025[a]	0.003	0.035[a]
$^2P^o_{3/2} - {}^2S_{1/2}$	0.763	0.740	0.840	1.067	1.110

excitation threshold, brought in by orbitals of correlation type, show up even more drastically in the effective collision strengths. A comparison between our results , tabulated in Table 6, and TH88 can be made in the T_e range $4\,10^5\,K - 3\,10^6\,K$. The two sets of effective collision strengths have the same trend as a function of T_e, with the noticeable exception of the 6 transitions marked by the superscript [b] in Table 6. For these transitions our Υ's increase with T_e, whereas Υ's in TH88 fall off with T_e, which is surprising considering that these are all optically allowed transitions and, most importantly, that for both sets of calculations the corresponding Ω's increase with E above 6.6 Ry. The large drop in Ω between 4 Ry and 6.6 Ry, mentioned above, almost certainly accounts for this unusual behaviour resulting from the integration of the collision strengths over a Maxwellian function. Further support for this hypothesis is offered by the $3s^2\,3p^3\ {}^2P^o_{3/2} \rightarrow 3s\,3p^4\ {}^2S_{1/2}$ transition ([c] in Table 6), which in TH88 shows a drop of almost a factor of 2 in the collision strength between 4 Ry and 6.6 Ry (their Table 2). This is clearly reflected in the drop of the effective collision strength at the lowest three temperatures tabulated in their Table 3. Starting from $T_e = 10^6$ K onwards the expected increase of Υ with T_e is otherwise correctly reproduced. If we make a numerical comparison of the two sets of data, we find that 69% (at $4\,10^5$ K) and 40% (at $3\,10^6$ K) of transitions differ by more than 50%, as shown by a superscript [a] in Table 6. We also note that

Table 5. Collision strengths for all electric dipole fine-structure transitions between the ground $3s^2\,3p^3$ and the second excited $3s^2\,3p^2\,3d$ configurations in Fe XII. [a] and [b] see text

Transition	$E = 6.6$ (Ry)		Transition	$E = 6.6$ (Ry)	
($3s^2\,3p^3 \rightarrow 3s^2\,3p^2\,3d$)	present work	Flower (1977)	($3s^2\,3p^3 \rightarrow 3s^2\,3p^2\,3d$)	present work	Flower (1977)
$^4S^o_{3/2} - (^3P)\,^4F_{3/2}$	0.035	0.033	$^2D^o_{5/2} - (^1D)\,^2F_{7/2}$	0.061	0.057
$^4S^o_{3/2} - (^3P)\,^4F_{5/2}$	0.050	0.047	$^2D^o_{5/2} - (^1D)\,^2G_{7/2}$	0.074	0.069
$^4S^o_{3/2} - (^1D)\,^2F_{5/2}$	0.038	0.025	$^2D^o_{5/2} - (^3P)\,^2P_{3/2}$	2.775	3.450
$^4S^o_{3/2} - (^3P)\,^4D_{1/2}$	0.007	0.006	$^2D^o_{5/2} - (^3P)\,^4P_{5/2}$	0.113	0.110
$^4S^o_{3/2} - (^3P)\,^4D_{3/2}$	0.025	0.023	$^2D^o_{5/2} - (^3P)\,^4P_{3/2}$	0.036	0.037
$^4S^o_{3/2} - (^3P)\,^4D_{5/2}$	0.026	0.037	$^2D^o_{5/2} - (^1S)\,^2D_{3/2}$	0.281	0.490[a]
$^4S^o_{3/2} - (^3P)\,^2P_{3/2}$	0.017	0.100[a]	$^2D^o_{5/2} - (^1S)\,^2D_{5/2}$	1.840	1.460
$^4S^o_{3/2} - (^3P)\,^4P_{5/2}$	5.089	6.600	$^2D^o_{5/2} - (^1D)\,^2D_{3/2}$	0.416	0.400
$^4S^o_{3/2} - (^3P)\,^2P_{1/2}$	0.056	0.790[a]	$^2D^o_{5/2} - (^1D)\,^2D_{5/2}$	2.673	4.450[a]
$^4S^o_{3/2} - (^3P)\,^4P_{3/2}$	3.397	3.950	$^2D^o_{5/2} - (^3P)\,^2F_{5/2}$	0.324	0.064[b]
$^4S^o_{3/2} - (^3P)\,^4P_{1/2}$	1.698	1.510	$^2D^o_{5/2} - (^1D)\,^2P_{3/2}$	0.049	0.280[a]
$^4S^o_{3/2} - (^1S)\,^2D_{3/2}$	0.118	0.540[a]	$^2D^o_{5/2} - (^3P)\,^2F_{7/2}$	7.027	9.130
$^4S^o_{3/2} - (^1S)\,^2D_{5/2}$	0.122	0.150	$^2D^o_{5/2} - (^3P)\,^2D_{5/2}$	0.217	0.740[b]
$^4S^o_{3/2} - (^1D)\,^2D_{3/2}$	0.001	0.001	$^2D^o_{5/2} - (^3P)\,^2D_{3/2}$	0.023	0.021
$^4S^o_{3/2} - (^1D)\,^2D_{5/2}$	0.005	0.009[a]	$^2P^o_{1/2} - (^3P)\,^4F_{3/2}$	0.009	0.007
$^4S^o_{3/2} - (^1D)\,^2P_{1/2}$	0.001	0.005[b]	$^2P^o_{1/2} - (^3P)\,^4D_{1/2}$	0.011	0.008
$^4S^o_{3/2} - (^3P)\,^2F_{5/2}$	0.033	0.026[b]	$^2P^o_{1/2} - (^3P)\,^4D_{3/2}$	0.014	0.012
$^4S^o_{3/2} - (^1D)\,^2P_{3/2}$	0.007	0.008	$^2P^o_{1/2} - (^3P)\,^2P_{3/2}$	0.120	0.050[a]
$^4S^o_{3/2} - (^1D)\,^2S_{1/2}$	0.005	0.0009[b]	$^2P^o_{1/2} - (^3P)\,^2P_{1/2}$	0.299	0.052[a]
$^4S^o_{3/2} - (^3P)\,^2D_{5/2}$	0.022	0.033[b]	$^2P^o_{1/2} - (^3P)\,^4P_{3/2}$	0.004	0.009[a]
$^4S^o_{3/2} - (^3P)\,^2D_{3/2}$	0.008	0.008	$^2P^o_{1/2} - (^3P)\,^4P_{1/2}$	0.012	0.031[a]
$^2D^o_{3/2} - (^3P)\,^4F_{3/2}$	0.051	0.046	$^2P^o_{1/2} - (^1S)\,^2D_{3/2}$	0.014	0.014
$^2D^o_{3/2} - (^3P)\,^4F_{5/2}$	0.048	0.043	$^2P^o_{1/2} - (^1D)\,^2D_{3/2}$	0.313	0.127[a]
$^2D^o_{3/2} - (^1D)\,^2F_{5/2}$	0.022	0.038[a]	$^2P^o_{1/2} - (^1D)\,^2P_{1/2}$	0.005	1.630[b]
$^2D^o_{3/2} - (^3P)\,^4D_{1/2}$	0.025	0.023	$^2P^o_{1/2} - (^1D)\,^2P_{3/2}$	0.762	0.850
$^2D^o_{3/2} - (^3P)\,^4D_{3/2}$	0.015	0.013	$^2P^o_{1/2} - (^1D)\,^2S_{1/2}$	1.392	0.310[b]
$^2D^o_{3/2} - (^3P)\,^4D_{5/2}$	0.038	0.020	$^2P^o_{1/2} - (^3P)\,^2D_{3/2}$	2.379	3.240
$^2D^o_{3/2} - (^3P)\,^2P_{3/2}$	1.077	1.070	$^2P^o_{3/2} - (^3P)\,^4F_{3/2}$	0.003	0.003
$^2D^o_{3/2} - (^3P)\,^4P_{5/2}$	0.044	0.056	$^2P^o_{3/2} - (^3P)\,^4F_{5/2}$	0.007	0.006
$^2D^o_{3/2} - (^3P)\,^2P_{1/2}$	1.182	1.190	$^2P^o_{3/2} - (^1D)\,^2F_{5/2}$	0.033	0.005[a]
$^2D^o_{3/2} - (^3P)\,^4P_{3/2}$	0.018	0.140[a]	$^2P^o_{3/2} - (^3P)\,^4D_{1/2}$	0.015	0.012
$^2D^o_{3/2} - (^3P)\,^4P_{1/2}$	0.065	0.490[a]	$^2P^o_{3/2} - (^3P)\,^4D_{3/2}$	0.018	0.014
$^2D^o_{3/2} - (^1S)\,^2D_{3/2}$	0.396	0.230	$^2P^o_{3/2} - (^3P)\,^4D_{5/2}$	0.007	0.029[a]
$^2D^o_{3/2} - (^1S)\,^2D_{5/2}$	0.057	0.079	$^2P^o_{3/2} - (^3P)\,^2P_{3/2}$	0.369	0.064[a]
$^2D^o_{3/2} - (^1D)\,^2D_{3/2}$	2.284	3.510[a]	$^2P^o_{3/2} - (^3P)\,^4P_{5/2}$	0.011	0.017[a]
$^2D^o_{3/2} - (^1D)\,^2D_{5/2}$	0.137	0.350[a]	$^2P^o_{3/2} - (^3P)\,^2P_{1/2}$	0.556	0.270[a]
$^2D^o_{3/2} - (^1D)\,^2P_{1/2}$	0.161	0.024[b]	$^2P^o_{3/2} - (^3P)\,^4P_{3/2}$	0.017	0.023
$^2D^o_{3/2} - (^3P)\,^2F_{5/2}$	4.948	0.029[b]	$^2P^o_{3/2} - (^3P)\,^4P_{1/2}$	0.015	0.190[a]
$^2D^o_{3/2} - (^1D)\,^2P_{3/2}$	0.066	0.100[a]	$^2P^o_{3/2} - (^1S)\,^2D_{3/2}$	0.056	0.049
$^2D^o_{3/2} - (^1D)\,^2S_{1/2}$	0.048	0.130[b]	$^2P^o_{3/2} - (^1S)\,^2D_{5/2}$	0.235	0.100[a]
$^2D^o_{3/2} - (^3P)\,^2D_{5/2}$	0.016	6.170[b]	$^2P^o_{3/2} - (^1D)\,^2D_{3/2}$	0.026	0.030
$^2D^o_{3/2} - (^3P)\,^2D_{3/2}$	0.017	0.047[a]	$^2P^o_{3/2} - (^1D)\,^2D_{5/2}$	0.406	0.380
$^2D^o_{5/2} - (^3P)\,^4F_{3/2}$	0.004	0.003	$^2P^o_{3/2} - (^1D)\,^2P_{1/2}$	1.302	0.440[b]
$^2D^o_{5/2} - (^3P)\,^4F_{5/2}$	0.021	0.022	$^2P^o_{3/2} - (^3P)\,^2F_{5/2}$	0.024	6.280[b]
$^2D^o_{5/2} - (^3P)\,^4F_{7/2}$	0.045	0.045	$^2P^o_{3/2} - (^1D)\,^2P_{3/2}$	2.212	2.760
$^2D^o_{5/2} - (^1D)\,^2F_{5/2}$	0.044	0.061	$^2P^o_{3/2} - (^1D)\,^2S_{1/2}$	0.012	1.660[b]
$^2D^o_{5/2} - (^3P)\,^4D_{7/2}$	0.081	0.072	$^2P^o_{3/2} - (^3P)\,^2D_{5/2}$	4.801	0.031[b]
$^2D^o_{5/2} - (^3P)\,^4D_{3/2}$	0.043	0.038	$^2P^o_{3/2} - (^3P)\,^2D_{3/2}$	0.772	0.720
$^2D^o_{5/2} - (^3P)\,^4D_{5/2}$	0.065	0.041			

for all such transitions Υ(present work) $< \Upsilon$(TH88). This, along with the fact that significantly more transitions have been rejected at the lower T_e, where resonance effects are more likely to contribute in the integration, forces us to

Table 6. Effective collision strengths for all electric dipole fine-structure transitions between the ground $3s^2\,3p^3$ and the first excited $3s\,3p^4$ configurations in Fe XII. Temperatures in the range $4\,10^5$ K $- 3\,10^6$ K. [a], [b] and [c] see text

Transition	T_e (10^5 K)										
($3s^2\,3p^3 \rightarrow 3s\,3p^4$)	4	6	8	10	12	14	16	18	20	25	30
$^4S^o_{3/2} - {}^4P_{5/2}$	0.8614	0.8920	0.9203	0.9457	0.9688	0.9898	1.0090	1.0270	1.0440	1.0820	1.1150
$^4S^o_{3/2} - {}^4P_{3/2}$	0.5652	0.5835	0.6009	0.6167	0.6312	0.6445	0.6568	0.6683	0.6790	0.7034	0.7248
$^4S^o_{3/2} - {}^4P_{1/2}$	0.2837	0.2930	0.3018	0.3098	0.3171	0.3238	0.3299	0.3357	0.3411	0.3533	0.3640
$^4S^o_{3/2} - {}^2D_{3/2}$	0.0049[a]	0.0045	0.0042	0.0040	0.0038	0.0037	0.0036	0.0034	0.0033	0.0031	0.0030[a]
$^4S^o_{3/2} - {}^2D_{5/2}$	0.0045[a]	0.0039	0.0036	0.0034	0.0033	0.0032	0.0031	0.0031	0.0031	0.0030	0.0030[a]
$^4S^o_{3/2} - {}^2P_{3/2}$	0.0771	0.0716	0.0675	0.0641	0.0612	0.0587	0.0565	0.0545	0.0527	0.0488	0.0456
$^4S^o_{3/2} - {}^2P_{1/2}$	0.0264	0.0244	0.0230	0.0219	0.0209	0.0201	0.0194	0.0188	0.0182	0.0170	0.0161
$^4S^o_{3/2} - {}^2S_{1/2}$	0.0124[a]	0.0120	0.0116	0.0113	0.0111	0.0109	0.0107	0.0106	0.0104	0.0101	0.0099[a]
$^2D^o_{3/2} - {}^4P_{5/2}$	0.0457[a]	0.0418	0.0394	0.0376	0.0362	0.0351	0.0342	0.0334	0.0327	0.0313	0.0302
$^2D^o_{3/2} - {}^4P_{3/2}$	0.0331[a]	0.0289	0.0262	0.0242	0.0226	0.0213	0.0202	0.0192	0.0183	0.0166	0.0152[a]
$^2D^o_{3/2} - {}^4P_{1/2}$	0.0163[a]	0.0142	0.0129	0.0120	0.0112	0.0106	0.0101	0.0097	0.0093	0.0085	0.0080
$^2D^o_{3/2} - {}^2D_{3/2}$	0.8267	0.8769	0.9183	0.9535	0.9841	1.0110	1.0360	1.0590	1.0790	1.1260	1.1660
$^2D^o_{3/2} - {}^2D_{5/2}$	0.0844[a]	0.0758	0.0703	0.0664	0.0633	0.0609	0.0589	0.0571	0.0556	0.0525	0.0502[a]
$^2D^o_{3/2} - {}^2P_{3/2}$[b]	0.1869[a]	0.1856	0.1869	0.1892	0.1918	0.1946	0.1973	0.2000	0.2026	0.2088	0.2145
$^2D^o_{3/2} - {}^2P_{1/2}$	0.5174	0.5445	0.5672	0.5869	0.6045	0.6204	0.6349	0.6484	0.6610	0.6893	0.7141
$^2D^o_{3/2} - {}^2S_{1/2}$	0.0463[a]	0.0441	0.0432	0.0429	0.0428	0.0429	0.0430	0.0432	0.0435	0.0441	0.0448[a]
$^2D^o_{5/2} - {}^4P_{5/2}$	0.0824[a]	0.0757	0.0715	0.0685	0.0662	0.0643	0.0628	0.0615	0.0603	0.0580	0.0563
$^2D^o_{5/2} - {}^4P_{3/2}$	0.0305[a]	0.0262	0.0235	0.0217	0.0203	0.0191	0.0182	0.0174	0.0167	0.0154	0.0143
$^2D^o_{5/2} - {}^2D_{3/2}$	0.1041[a]	0.0922	0.0848	0.0796	0.0756	0.0724	0.0697	0.0674	0.0655	0.0615	0.0584[a]
$^2D^o_{5/2} - {}^2D_{5/2}$	1.1570	1.2060	1.2500	1.2890	1.3230	1.3540	1.3830	1.4090	1.4330	1.4880	1.5360
$^2D^o_{5/2} - {}^2P_{3/2}$	1.2540	1.3060	1.3530	1.3950	1.4320	1.4670	1.4990	1.5280	1.5560	1.6190	1.6740
$^2P^o_{1/2} - {}^4P_{3/2}$	0.0213[a]	0.0188	0.0171	0.0159	0.0149	0.0141	0.0133	0.0127	0.0122	0.0110	0.0101[a]
$^2P^o_{1/2} - {}^4P_{1/2}$	0.0170[a]	0.0163	0.0157	0.0152	0.0148	0.0145	0.0142	0.0139	0.0136	0.0131	0.0127
$^2P^o_{1/2} - {}^2D_{3/2}$[b]	0.1308[a]	0.1312	0.1330	0.1352	0.1375	0.1396	0.1417	0.1437	0.1456	0.1499	0.1538
$^2P^o_{1/2} - {}^2P_{3/2}$[b]	0.0932[a]	0.0945	0.0962	0.0978	0.0994	0.1010	0.1024	0.1038	0.1051	0.1081	0.1108
$^2P^o_{1/2} - {}^2P_{1/2}$	0.3362[a]	0.3600	0.3782	0.3932	0.4061	0.4175	0.4277	0.4371	0.4457	0.4648	0.4812
$^2P^o_{1/2} - {}^2S_{1/2}$[b]	0.0742	0.0779	0.0810	0.0837	0.0861	0.0883	0.0903	0.0922	0.0940	0.0979	0.1014[a]
$^2P^o_{3/2} - {}^4P_{5/2}$	0.0480[a]	0.0413	0.0371	0.0342	0.0320	0.0302	0.0288	0.0275	0.0265	0.0243	0.0227[a]
$^2P^o_{3/2} - {}^4P_{3/2}$	0.0440[a]	0.0400	0.0375	0.0356	0.0342	0.0331	0.0322	0.0314	0.0306	0.0292	0.0281[a]
$^2P^o_{3/2} - {}^4P_{1/2}$	0.0222[a]	0.0192	0.0174	0.0160	0.0150	0.0141	0.0134	0.0128	0.0122	0.0111	0.0103[a]
$^2P^o_{3/2} - {}^2D_{3/2}$	0.0719[a]	0.0617	0.0557	0.0516	0.0487	0.0463	0.0445	0.0429	0.0416	0.0391	0.0372[a]
$^2P^o_{3/2} - {}^2D_{5/2}$[b]	0.3843[a]	0.3927	0.4026	0.4122	0.4211	0.4293	0.4370	0.4441	0.4507	0.4657	0.4789
$^2P^o_{3/2} - {}^2P_{3/2}$[b]	0.1752[a]	0.1783	0.1820	0.1857	0.1892	0.1925	0.1956	0.1985	0.2012	0.2075	0.2131
$^2P^o_{3/2} - {}^2P_{1/2}$	0.0377[a]	0.0287	0.0238	0.0206	0.0183	0.0166	0.0152	0.0141	0.0132	0.0114	0.0101[a]
$^2P^o_{3/2} - {}^2S_{1/2}$[c]	0.7153	0.7455	0.7716	0.7944	0.8148	0.8333	0.8504	0.8662	0.8810	0.9143	0.9436

believe once more that the reason for the large Υ values in TH88 lies in pseudo-resonance contributions due to the use of correlation orbitals in the target description.

3.2. $3s^2\,3p^3 - 3s^2\,3p^2\,3d$ transitions

The only set of $3s^2\,3p^3 \rightarrow 3s^2\,3p^2\,3d$ electric dipole collision strengths available for comparison with the present work is by F77. Given the limitations of that computation, discussed above, we believe that our much more comprehensive target representation, proper inclusion and treatment of resonances and the provision of collisional data over a wide energy range represent the major new component of the present results. Out of 97 transitions 42 have not been included in the analysis, 16 (marked with [b] in Table 5) because of presumed identification problems to be discussed later and 26 (marked with [a] in Table 5) as not satisfying the $\pm 50\%$ criterion introduced above. For the remaining transitions we get an average difference of 16.5% between the two sets of data. We point out that of these 26 transitions marked with [a], 11 have $\Omega > 0.1$, 5

Table 7. Effective collision strengths for all electric dipole fine-structure transitions between the ground $3s^2\,3p^3$ and the first excited $3s\,3p^4$ configurations in Fe XII. Temperatures in the range $4\,10^6$ K $- 10^7$ K

Transition	T_e (10^6 K)						
($3s^2\,3p^3 \rightarrow 3s\,3p^4$)	4	5	6	7	8	9	10
$^4S^o_{3/2} - {}^4P_{5/2}$	1.1720	1.2190	1.2590	1.2950	1.3260	1.3550	1.3810
$^4S^o_{3/2} - {}^4P_{3/2}$	0.7613	0.7918	0.8180	0.8410	0.8615	0.8800	0.8969
$^4S^o_{3/2} - {}^4P_{1/2}$	0.3823	0.3976	0.4107	0.4223	0.4325	0.4418	0.4502
$^4S^o_{3/2} - {}^2D_{3/2}$	0.0028	0.0026	0.0025	0.0024	0.0023	0.0022	0.0022
$^4S^o_{3/2} - {}^2D_{5/2}$	0.0030	0.0031	0.0031	0.0032	0.0032	0.0032	0.0033
$^4S^o_{3/2} - {}^2P_{3/2}$	0.0408	0.0372	0.0344	0.0322	0.0304	0.0289	0.0277
$^4S^o_{3/2} - {}^2P_{1/2}$	0.0146	0.0135	0.0127	0.0120	0.0115	0.0110	0.0107
$^4S^o_{3/2} - {}^2S_{1/2}$	0.0095	0.0093	0.0091	0.0090	0.0089	0.0088	0.0088
$^2D^o_{3/2} - {}^4P_{5/2}$	0.0287	0.0277	0.0269	0.0264	0.0260	0.0257	0.0254
$^2D^o_{3/2} - {}^4P_{3/2}$	0.0132	0.0117	0.0106	0.0098	0.0091	0.0085	0.0080
$^2D^o_{3/2} - {}^4P_{1/2}$	0.0071	0.0065	0.0060	0.0057	0.0054	0.0051	0.0049
$^2D^o_{3/2} - {}^2D_{3/2}$	1.2330	1.2870	1.3340	1.3750	1.4110	1.4430	1.4730
$^2D^o_{3/2} - {}^2D_{5/2}$	0.0468	0.0445	0.0428	0.0415	0.0404	0.0397	0.0390
$^2D^o_{3/2} - {}^2P_{3/2}$	0.2247	0.2334	0.2410	0.2477	0.2537	0.2592	0.2642
$^2D^o_{3/2} - {}^2P_{1/2}$	0.7561	0.7910	0.8208	0.8469	0.8702	0.8911	0.9101
$^2D^o_{3/2} - {}^2S_{1/2}$	0.0460	0.0472	0.0483	0.0492	0.0501	0.0510	0.0517
$^2D^o_{5/2} - {}^4P_{5/2}$	0.0539	0.0522	0.0511	0.0503	0.0497	0.0492	0.0489
$^2D^o_{5/2} - {}^4P_{3/2}$	0.0128	0.0118	0.0110	0.0104	0.0100	0.0096	0.0093
$^2D^o_{5/2} - {}^2D_{3/2}$	0.0540	0.0510	0.0487	0.0470	0.0457	0.0446	0.0438
$^2D^o_{5/2} - {}^2D_{5/2}$	1.6160	1.6830	1.7400	1.7900	1.8350	1.8750	1.9110
$^2D^o_{5/2} - {}^2P_{3/2}$	1.7680	1.8460	1.9140	1.9720	2.0250	2.0720	2.1150
$^2P^o_{1/2} - {}^4P_{3/2}$	0.0088	0.0078	0.0070	0.0064	0.0059	0.0055	0.0052
$^2P^o_{1/2} - {}^4P_{1/2}$	0.0121	0.0116	0.0112	0.0110	0.0108	0.0106	0.0105
$^2P^o_{1/2} - {}^2D_{3/2}$	0.1605	0.1662	0.1711	0.1755	0.1794	0.1829	0.1862
$^2P^o_{1/2} - {}^2P_{3/2}$	0.1155	0.1195	0.1230	0.1262	0.1289	0.1315	0.1338
$^2P^o_{1/2} - {}^2P_{1/2}$	0.5087	0.5312	0.5503	0.5669	0.5816	0.5949	0.6069
$^2P^o_{1/2} - {}^2S_{1/2}$	0.1073	0.1121	0.1163	0.1199	0.1231	0.1260	0.1287
$^2P^o_{3/2} - {}^4P_{5/2}$	0.0203	0.0186	0.0174	0.0164	0.0157	0.0150	0.0145
$^2P^o_{3/2} - {}^4P_{3/2}$	0.0266	0.0255	0.0247	0.0242	0.0237	0.0234	0.0231
$^2P^o_{3/2} - {}^4P_{1/2}$	0.0090	0.0082	0.0075	0.0070	0.0065	0.0062	0.0059
$^2P^o_{3/2} - {}^2D_{3/2}$	0.0345	0.0327	0.0314	0.0305	0.0298	0.0292	0.0287
$^2P^o_{3/2} - {}^2D_{5/2}$	0.5012	0.5198	0.5357	0.5497	0.5622	0.5734	0.5836
$^2P^o_{3/2} - {}^2P_{3/2}$	0.2227	0.2308	0.2378	0.2439	0.2495	0.2545	0.2591
$^2P^o_{3/2} - {}^2P_{1/2}$	0.0084	0.0072	0.0063	0.0057	0.0052	0.0048	0.0044
$^2P^o_{3/2} - {}^2S_{1/2}$	0.9934	1.0350	1.0710	1.1020	1.1300	1.1550	1.1780

have $\Omega > 0.3$ and only 2 have $\Omega > 1$. Again, this clearly shows that the most severe errors, from a factor of 2 up to more than an order of magnitude, occur for low collision strength values, i.e. weak transitions where cancellation effects due to the particular target expansion are more likely to affect the final results.

The transitions marked by ^{b} in Table 5 deserve a separate discussion as we have evidence of label misassignment for the upper levels of these transitions in F77. The most striking case is for the two levels $(^3P)\,^2F_{5/2}$ and $(^3P)\,^2D_{5/2}$. By comparing the collision strength values for $^2D^o_{3/2} - (^3P)\,^2F_{5/2}$ and $^2D^o_{3/2} - (^3P)\,^2D_{5/2}$ in Table 5 it is evident that the relative strengths of these two transitions are reversed in the two calculations. By reassigning in F77 the higher collision strength to the former transition and the lower one to the latter we get a significant improvement in agreement from more than 2 orders of magnitude down to 25% and 81% (still a big difference, but this is a low Ω value, < 0.1!), respectively. Similarly for the $^2P^o_{3/2} - (^3P)\,^2F_{5/2}$, $^2P^o_{3/2} - (^3P)\,^2D_{5/2}$ transitions by interchanging the collision strengths in F77 the difference between the two sets of data drops from more than 2 orders of magnitude down to 29% and 31% respectively. The other suspected case of mislabelling is that of levels $(^1D)\,^2P_{1/2}$ and $(^1D)\,^2S_{1/2}$. The stronger transition in our computation is the $^2P^o_{1/2} - (^1D)\,^2S_{1/2}$ rather than the $^2P^o_{1/2} - (^1D)\,^2P_{1/2}$ as in F77. By reassigning the high Ω to the former transition in F77, the difference decreases from more than a factor of 4 down to 17%. Similarly, by interchanging the Ω's for the $^2P^o_{3/2} - (^1D)\,^2P_{1/2}$, $^2P^o_{3/2} - (^1D)\,^2S_{1/2}$ transitions in F77, we get a difference of 27.5%

Table 8. Effective collision strengths for all electric dipole fine-structure transitions between the ground $3s^2\,3p^3$ and the second excited $3s^2\,3p^2\,3d$ configurations in Fe XII. Temperatures in the range $4\,10^5$ K $- 3\,10^6$ K

Transition	T_e (10^5 K)										
($3s^2\,3p^3 \rightarrow 3s^2\,3p^2\,3d$)	4	6	8	10	12	14	16	18	20	25	30
$^4S^o_{3/2} - (^3P)\,^4F_{3/2}$	0.0470	0.0426	0.0401	0.0385	0.0373	0.0364	0.0357	0.0352	0.0347	0.0339	0.0333
$^4S^o_{3/2} - (^3P)\,^4F_{5/2}$	0.0684	0.0619	0.0584	0.0560	0.0544	0.0531	0.0522	0.0514	0.0508	0.0498	0.0490
$^4S^o_{3/2} - (^1D)\,^2F_{5/2}$	0.0378	0.0377	0.0377	0.0378	0.0379	0.0381	0.0382	0.0384	0.0386	0.0392	0.0398
$^4S^o_{3/2} - (^3P)\,^4D_{1/2}$	0.0082	0.0074	0.0069	0.0066	0.0063	0.0061	0.0059	0.0058	0.0056	0.0054	0.0052
$^4S^o_{3/2} - (^3P)\,^4D_{3/2}$	0.0258	0.0254	0.0252	0.0251	0.0250	0.0251	0.0251	0.0252	0.0253	0.0255	0.0258
$^4S^o_{3/2} - (^3P)\,^4D_{5/2}$	0.0280	0.0266	0.0257	0.0250	0.0245	0.0240	0.0236	0.0233	0.0230	0.0225	0.0221
$^4S^o_{3/2} - (^3P)\,^2P_{3/2}$	0.0172	0.0171	0.0170	0.0170	0.0171	0.0171	0.0172	0.0173	0.0173	0.0176	0.0178
$^4S^o_{3/2} - (^3P)\,^4P_{5/2}$	5.1850	5.3540	5.5130	5.6620	5.8030	5.9350	6.0610	6.1800	6.2940	6.5570	6.7940
$^4S^o_{3/2} - (^3P)\,^2P_{1/2}$	0.0550	0.0575	0.0596	0.0615	0.0632	0.0649	0.0665	0.0680	0.0695	0.0729	0.0760
$^4S^o_{3/2} - (^3P)\,^4P_{3/2}$	3.4660	3.5780	3.6830	3.7820	3.8750	3.9630	4.0470	4.1270	4.2020	4.3770	4.5350
$^4S^o_{3/2} - (^3P)\,^4P_{1/2}$	1.7320	1.7890	1.8410	1.8910	1.9370	1.9810	2.0230	2.0630	2.1000	2.1880	2.2660
$^4S^o_{3/2} - (^1S)\,^2D_{3/2}$	0.1213	0.1244	0.1273	0.1302	0.1329	0.1355	0.1381	0.1405	0.1427	0.1481	0.1530
$^4S^o_{3/2} - (^1S)\,^2D_{5/2}$	0.1253	0.1285	0.1316	0.1347	0.1376	0.1403	0.1430	0.1455	0.1479	0.1536	0.1588
$^4S^o_{3/2} - (^1D)\,^2D_{3/2}$	0.0011	0.0009	0.0008	0.0008	0.0007	0.0007	0.0006	0.0006	0.0006	0.0005	0.0005
$^4S^o_{3/2} - (^1D)\,^2D_{5/2}$	0.0051	0.0052	0.0054	0.0055	0.0056	0.0057	0.0058	0.0059	0.0060	0.0062	0.0063
$^4S^o_{3/2} - (^1D)\,^2P_{1/2}$	0.0012	0.0011	0.0010	0.0009	0.0009	0.0008	0.0008	0.0008	0.0007	0.0007	0.0006
$^4S^o_{3/2} - (^3P)\,^2F_{5/2}$	0.0304	0.0300	0.0295	0.0290	0.0286	0.0282	0.0278	0.0275	0.0273	0.0267	0.0263
$^4S^o_{3/2} - (^1D)\,^2P_{3/2}$	0.0074	0.0070	0.0066	0.0063	0.0061	0.0058	0.0056	0.0055	0.0053	0.0050	0.0048
$^4S^o_{3/2} - (^1D)\,^2S_{1/2}$	0.0045	0.0042	0.0040	0.0038	0.0037	0.0036	0.0034	0.0033	0.0032	0.0030	0.0029
$^4S^o_{3/2} - (^3P)\,^2D_{5/2}$	0.0220	0.0217	0.0214	0.0213	0.0212	0.0212	0.0211	0.0211	0.0211	0.0212	0.0213
$^4S^o_{3/2} - (^3P)\,^2D_{3/2}$	0.0073	0.0069	0.0066	0.0064	0.0061	0.0059	0.0058	0.0056	0.0055	0.0052	0.0050
$^2D^o_{3/2} - (^3P)\,^4F_{3/2}$	0.0588	0.0550	0.0524	0.0505	0.0489	0.0476	0.0465	0.0456	0.0448	0.0432	0.0419
$^2D^o_{3/2} - (^3P)\,^4F_{5/2}$	0.0639	0.0568	0.0521	0.0485	0.0457	0.0433	0.0413	0.0396	0.0380	0.0348	0.0323
$^2D^o_{3/2} - (^1D)\,^2F_{5/2}$	0.0401	0.0339	0.0302	0.0278	0.0260	0.0247	0.0236	0.0227	0.0219	0.0204	0.0194
$^2D^o_{3/2} - (^3P)\,^4D_{1/2}$	0.0276	0.0270	0.0268	0.0267	0.0268	0.0268	0.0269	0.0270	0.0271	0.0274	0.0278
$^2D^o_{3/2} - (^3P)\,^4D_{3/2}$	0.0246	0.0208	0.0185	0.0169	0.0156	0.0146	0.0137	0.0130	0.0124	0.0111	0.0101
$^2D^o_{3/2} - (^3P)\,^4D_{5/2}$	0.0706	0.0601	0.0542	0.0504	0.0477	0.0457	0.0441	0.0429	0.0419	0.0400	0.0386
$^2D^o_{3/2} - (^3P)\,^2P_{3/2}$	1.0500	1.0990	1.1390	1.1740	1.2060	1.2350	1.2620	1.2880	1.3120	1.3680	1.4170
$^2D^o_{3/2} - (^3P)\,^4P_{5/2}$	0.0589	0.0541	0.0514	0.0497	0.0485	0.0478	0.0472	0.0468	0.0465	0.0461	0.0460
$^2D^o_{3/2} - (^3P)\,^2P_{1/2}$	1.1860	1.2300	1.2690	1.3060	1.3390	1.3710	1.4010	1.4290	1.4550	1.5160	1.5710
$^2D^o_{3/2} - (^3P)\,^4P_{3/2}$	0.0251	0.0229	0.0218	0.0212	0.0208	0.0205	0.0203	0.0202	0.0201	0.0200	0.0200
$^2D^o_{3/2} - (^3P)\,^4P_{1/2}$	0.0755	0.0746	0.0750	0.0759	0.0771	0.0783	0.0796	0.0809	0.0821	0.0853	0.0882
$^2D^o_{3/2} - (^1S)\,^2D_{3/2}$	0.4214	0.4294	0.4390	0.4488	0.4585	0.4679	0.4769	0.4855	0.4938	0.5130	0.5304
$^2D^o_{3/2} - (^1S)\,^2D_{5/2}$	0.0604	0.0612	0.0623	0.0634	0.0645	0.0657	0.0667	0.0678	0.0688	0.0712	0.0734
$^2D^o_{3/2} - (^1D)\,^2D_{3/2}$	2.3700	2.4440	2.5140	2.5810	2.6440	2.7040	2.7610	2.8150	2.8670	2.9860	3.0930
$^2D^o_{3/2} - (^1D)\,^2D_{5/2}$	0.1344	0.1391	0.1430	0.1465	0.1497	0.1527	0.1555	0.1582	0.1607	0.1667	0.1721
$^2D^o_{3/2} - (^1D)\,^2P_{1/2}$	0.1682	0.1731	0.1778	0.1823	0.1865	0.1905	0.1943	0.1979	0.2013	0.2091	0.2162
$^2D^o_{3/2} - (^3P)\,^2F_{5/2}$	5.0850	5.2770	5.4500	5.6080	5.7570	5.8960	6.0270	6.1510	6.2700	6.5420	6.7870
$^2D^o_{3/2} - (^1D)\,^2P_{3/2}$	0.0680	0.0688	0.0697	0.0706	0.0715	0.0724	0.0733	0.0741	0.0749	0.0768	0.0786
$^2D^o_{3/2} - (^1D)\,^2S_{1/2}$	0.0501	0.0510	0.0520	0.0530	0.0540	0.0549	0.0559	0.0568	0.0576	0.0597	0.0615
$^2D^o_{3/2} - (^3P)\,^2D_{5/2}$	0.0200	0.0182	0.0172	0.0165	0.0160	0.0156	0.0153	0.0150	0.0148	0.0144	0.0141
$^2D^o_{3/2} - (^3P)\,^2D_{3/2}$	0.0265	0.0233	0.0217	0.0207	0.0201	0.0197	0.0193	0.0191	0.0189	0.0187	0.0185
$^2D^o_{5/2} - (^3P)\,^4F_{3/2}$	0.0101	0.0080	0.0068	0.0060	0.0054	0.0050	0.0046	0.0043	0.0041	0.0036	0.0032
$^2D^o_{5/2} - (^3P)\,^4F_{5/2}$	0.0324	0.0286	0.0262	0.0247	0.0235	0.0226	0.0218	0.0212	0.0207	0.0197	0.0190
$^2D^o_{5/2} - (^3P)\,^4F_{7/2}$	0.0666	0.0582	0.0528	0.0490	0.0460	0.0436	0.0415	0.0398	0.0382	0.0351	0.0327
$^2D^o_{5/2} - (^1D)\,^2F_{5/2}$	0.0633	0.0562	0.0520	0.0491	0.0470	0.0453	0.0439	0.0428	0.0418	0.0399	0.0386
$^2D^o_{5/2} - (^3P)\,^4D_{7/2}$	0.1327	0.1146	0.1040	0.0969	0.0917	0.0877	0.0844	0.0818	0.0795	0.0751	0.0719
$^2D^o_{5/2} - (^3P)\,^4D_{3/2}$	0.0470	0.0459	0.0454	0.0452	0.0451	0.0452	0.0452	0.0454	0.0455	0.0460	0.0465
$^2D^o_{5/2} - (^3P)\,^4D_{5/2}$	0.1043	0.0900	0.0814	0.0754	0.0709	0.0673	0.0643	0.0619	0.0597	0.0554	0.0522

Table 8. continued

Transition	T_e (10^5 K)										
($3s^2\,3p^3 \rightarrow 3s^2\,3p^2\,3d$)	4	6	8	10	12	14	16	18	20	25	30
$^2D^o_{5/2} - (^1D)\,^2F_{7/2}$	0.1120	0.0949	0.0851	0.0787	0.0740	0.0705	0.0677	0.0654	0.0634	0.0598	0.0571
$^2D^o_{5/2} - (^1D)\,^2G_{7/2}$	0.0948	0.0862	0.0812	0.0779	0.0755	0.0736	0.0722	0.0710	0.0700	0.0682	0.0670
$^2D^o_{5/2} - (^3P)\,^2P_{3/2}$	2.8410	2.9230	3.0040	3.0800	3.1530	3.2220	3.2870	3.3490	3.4080	3.5440	3.6660
$^2D^o_{5/2} - (^3P)\,^4P_{5/2}$	0.1239	0.1229	0.1233	0.1241	0.1253	0.1266	0.1279	0.1293	0.1307	0.1341	0.1374
$^2D^o_{5/2} - (^3P)\,^4P_{3/2}$	0.0423	0.0397	0.0381	0.0371	0.0363	0.0358	0.0353	0.0350	0.0347	0.0343	0.0341
$^2D^o_{5/2} - (^1S)\,^2D_{3/2}$	0.2907	0.2985	0.3062	0.3137	0.3209	0.3277	0.3342	0.3404	0.3463	0.3601	0.3725
$^2D^o_{5/2} - (^1S)\,^2D_{5/2}$	1.8590	1.9300	1.9940	2.0520	2.1060	2.1560	2.2040	2.2490	2.2920	2.3900	2.4780
$^2D^o_{5/2} - (^1D)\,^2D_{3/2}$	0.4322	0.4428	0.4534	0.4637	0.4736	0.4831	0.4921	0.5008	0.5090	0.5283	0.5458
$^2D^o_{5/2} - (^1D)\,^2D_{5/2}$	2.7760	2.8600	2.9420	3.0200	3.0930	3.1630	3.2300	3.2930	3.3540	3.4930	3.6190
$^2D^o_{5/2} - (^3P)\,^2F_{5/2}$	0.3703	0.3678	0.3701	0.3742	0.3791	0.3843	0.3896	0.3949	0.4002	0.4128	0.4246
$^2D^o_{5/2} - (^1D)\,^2P_{3/2}$	0.0502	0.0500	0.0501	0.0503	0.0505	0.0508	0.0511	0.0514	0.0517	0.0525	0.0533
$^2D^o_{5/2} - (^3P)\,^2F_{7/2}$	7.3750	7.5980	7.8170	8.0250	8.2240	8.4130	8.5930	8.7650	8.9280	9.3070	9.6490
$^2D^o_{5/2} - (^3P)\,^2D_{5/2}$	0.3200	0.2958	0.2860	0.2819	0.2807	0.2810	0.2822	0.2840	0.2861	0.2922	0.2986
$^2D^o_{5/2} - (^3P)\,^2D_{3/2}$	0.0521	0.0430	0.0384	0.0356	0.0338	0.0325	0.0316	0.0309	0.0304	0.0295	0.0290
$^2P^o_{1/2} - (^3P)\,^4F_{3/2}$	0.0150	0.0128	0.0115	0.0107	0.0100	0.0095	0.0091	0.0087	0.0085	0.0079	0.0075
$^2P^o_{1/2} - (^3P)\,^4D_{1/2}$	0.0136	0.0123	0.0115	0.0109	0.0104	0.0100	0.0097	0.0094	0.0091	0.0086	0.0082
$^2P^o_{1/2} - (^3P)\,^4D_{3/2}$	0.0205	0.0180	0.0164	0.0152	0.0142	0.0135	0.0128	0.0122	0.0117	0.0107	0.0099
$^2P^o_{1/2} - (^3P)\,^2P_{3/2}$	0.1343	0.1337	0.1347	0.1364	0.1383	0.1403	0.1422	0.1442	0.1461	0.1506	0.1548
$^2P^o_{1/2} - (^3P)\,^2P_{1/2}$	0.2963	0.3078	0.3179	0.3270	0.3353	0.3430	0.3503	0.3571	0.3635	0.3781	0.3910
$^2P^o_{1/2} - (^3P)\,^4P_{3/2}$	0.0078	0.0064	0.0056	0.0050	0.0046	0.0042	0.0039	0.0037	0.0035	0.0031	0.0028
$^2P^o_{1/2} - (^3P)\,^4P_{1/2}$	0.0140	0.0137	0.0137	0.0137	0.0138	0.0140	0.0141	0.0142	0.0144	0.0147	0.0151
$^2P^o_{1/2} - (^1S)\,^2D_{3/2}$	0.0262	0.0215	0.0188	0.0169	0.0156	0.0145	0.0137	0.0129	0.0123	0.0111	0.0102
$^2P^o_{1/2} - (^1D)\,^2D_{3/2}$	0.3065	0.3212	0.3334	0.3440	0.3536	0.3624	0.3706	0.3783	0.3856	0.4021	0.4168
$^2P^o_{1/2} - (^1D)\,^2P_{1/2}$	0.0049	0.0048	0.0047	0.0046	0.0046	0.0047	0.0047	0.0047	0.0048	0.0049	0.0051
$^2P^o_{1/2} - (^1D)\,^2P_{3/2}$	0.7610	0.7967	0.8264	0.8527	0.8766	0.8988	0.9195	0.9389	0.9572	0.9990	1.0360
$^2P^o_{1/2} - (^1D)\,^2S_{1/2}$	1.4480	1.4970	1.5430	1.5860	1.6260	1.6650	1.7010	1.7350	1.7680	1.8440	1.9120
$^2P^o_{1/2} - (^3P)\,^2D_{3/2}$	2.4910	2.5760	2.6560	2.7310	2.8010	2.8680	2.9310	2.9910	3.0480	3.1800	3.2980
$^2P^o_{3/2} - (^3P)\,^4F_{3/2}$	0.0127	0.0099	0.0082	0.0071	0.0063	0.0057	0.0053	0.0049	0.0046	0.0040	0.0035
$^2P^o_{3/2} - (^3P)\,^4F_{5/2}$	0.0211	0.0168	0.0144	0.0129	0.0117	0.0109	0.0103	0.0097	0.0093	0.0084	0.0078
$^2P^o_{3/2} - (^1D)\,^2F_{5/2}$	0.0512	0.0442	0.0397	0.0364	0.0339	0.0318	0.0301	0.0286	0.0273	0.0247	0.0226
$^2P^o_{3/2} - (^3P)\,^4D_{1/2}$	0.0185	0.0176	0.0170	0.0167	0.0165	0.0164	0.0163	0.0162	0.0162	0.0162	0.0162
$^2P^o_{3/2} - (^3P)\,^4D_{3/2}$	0.0272	0.0239	0.0218	0.0203	0.0192	0.0183	0.0175	0.0169	0.0163	0.0152	0.0144
$^2P^o_{3/2} - (^3P)\,^4D_{5/2}$	0.0273	0.0210	0.0174	0.0151	0.0135	0.0122	0.0113	0.0105	0.0098	0.0086	0.0078
$^2P^o_{3/2} - (^3P)\,^2P_{3/2}$	0.3772	0.3865	0.3958	0.4048	0.4132	0.4212	0.4288	0.4359	0.4427	0.4584	0.4724
$^2P^o_{3/2} - (^3P)\,^4P_{5/2}$	0.0363	0.0280	0.0233	0.0203	0.0181	0.0165	0.0152	0.0141	0.0133	0.0116	0.0104
$^2P^o_{3/2} - (^3P)\,^2P_{1/2}$	0.5953	0.6032	0.6147	0.6271	0.6396	0.6519	0.6637	0.6751	0.6860	0.7115	0.7347
$^2P^o_{3/2} - (^3P)\,^4P_{3/2}$	0.0369	0.0305	0.0270	0.0249	0.0234	0.0224	0.0216	0.0210	0.0205	0.0197	0.0192
$^2P^o_{3/2} - (^3P)\,^4P_{1/2}$	0.0170	0.0164	0.0161	0.0160	0.0160	0.0160	0.0161	0.0161	0.0162	0.0165	0.0169
$^2P^o_{3/2} - (^1S)\,^2D_{3/2}$	0.0695	0.0652	0.0630	0.0618	0.0611	0.0606	0.0603	0.0602	0.0601	0.0602	0.0604
$^2P^o_{3/2} - (^1S)\,^2D_{5/2}$	0.2557	0.2556	0.2577	0.2606	0.2639	0.2673	0.2708	0.2742	0.2775	0.2856	0.2930
$^2P^o_{3/2} - (^1D)\,^2D_{3/2}$	0.0406	0.0356	0.0330	0.0315	0.0305	0.0298	0.0293	0.0289	0.0287	0.0283	0.0282
$^2P^o_{3/2} - (^1D)\,^2D_{5/2}$	0.4695	0.4652	0.4678	0.4730	0.4793	0.4861	0.4930	0.4999	0.5067	0.5231	0.5384
$^2P^o_{3/2} - (^1D)\,^2P_{1/2}$	1.3550	1.3980	1.4390	1.4780	1.5150	1.5490	1.5820	1.6130	1.6420	1.7100	1.7710
$^2P^o_{3/2} - (^3P)\,^2F_{5/2}$	0.1119	0.0846	0.0703	0.0616	0.0557	0.0515	0.0483	0.0459	0.0440	0.0405	0.0383
$^2P^o_{3/2} - (^1D)\,^2P_{3/2}$	2.3390	2.4030	2.4680	2.5310	2.5920	2.6500	2.7050	2.7580	2.8090	2.9250	3.0300
$^2P^o_{3/2} - (^1D)\,^2S_{1/2}$	0.0151	0.0138	0.0131	0.0127	0.0125	0.0124	0.0123	0.0122	0.0122	0.0122	0.0123
$^2P^o_{3/2} - (^3P)\,^2D_{5/2}$	5.0320	5.2000	5.3580	5.5060	5.6460	5.7790	5.9040	6.0230	6.1370	6.3990	6.6340
$^2P^o_{3/2} - (^3P)\,^2D_{3/2}$	0.8089	0.8346	0.8589	0.8818	0.9036	0.9241	0.9436	0.9621	0.9798	1.0210	1.0570

Table 9. Effective collision strengths for all electric dipole fine-structure transitions between the ground $3s^2\,3p^3$ and the second excited $3s^2\,3p^2\,3d$ configurations in Fe XII. Temperatures in the range $4\,10^6$ K $- 10^7$ K

Transition	T_e (10^6 K)						
($3s^2\,3p^3 \rightarrow 3s^2\,3p^2\,3d$)	4	5	6	7	8	9	10
$^4S^o_{3/2} - (^3P)\,^4F_{3/2}$	0.0326	0.0322	0.0320	0.0318	0.0318	0.0317	0.0316
$^4S^o_{3/2} - (^3P)\,^4F_{5/2}$	0.0482	0.0478	0.0476	0.0475	0.0475	0.0475	0.0475
$^4S^o_{3/2} - (^1D)\,^2F_{5/2}$	0.0409	0.0419	0.0429	0.0438	0.0447	0.0455	0.0462
$^4S^o_{3/2} - (^3P)\,^4D_{1/2}$	0.0049	0.0048	0.0047	0.0046	0.0045	0.0045	0.0045
$^4S^o_{3/2} - (^3P)\,^4D_{3/2}$	0.0264	0.0270	0.0276	0.0281	0.0286	0.0291	0.0295
$^4S^o_{3/2} - (^3P)\,^4D_{5/2}$	0.0216	0.0213	0.0212	0.0211	0.0211	0.0212	0.0212
$^4S^o_{3/2} - (^3P)\,^2P_{3/2}$	0.0183	0.0187	0.0192	0.0196	0.0200	0.0204	0.0207
$^4S^o_{3/2} - (^3P)\,^4P_{5/2}$	7.2070	7.5590	7.8650	8.1350	8.3780	8.5980	8.8000
$^4S^o_{3/2} - (^3P)\,^2P_{1/2}$	0.0815	0.0863	0.0905	0.0942	0.0976	0.1006	0.1034
$^4S^o_{3/2} - (^3P)\,^4P_{3/2}$	4.8110	5.0450	5.2490	5.4290	5.5910	5.7380	5.8720
$^4S^o_{3/2} - (^3P)\,^4P_{1/2}$	2.4030	2.5190	2.6210	2.7100	2.7900	2.8630	2.9300
$^4S^o_{3/2} - (^1S)\,^2D_{3/2}$	0.1616	0.1690	0.1756	0.1814	0.1866	0.1914	0.1958
$^4S^o_{3/2} - (^1S)\,^2D_{5/2}$	0.1679	0.1758	0.1827	0.1889	0.1944	0.1995	0.2042
$^4S^o_{3/2} - (^1D)\,^2D_{3/2}$	0.0005	0.0004	0.0004	0.0004	0.0004	0.0003	0.0003
$^4S^o_{3/2} - (^1D)\,^2D_{5/2}$	0.0067	0.0069	0.0072	0.0074	0.0076	0.0078	0.0080
$^4S^o_{3/2} - (^1D)\,^2P_{1/2}$	0.0005	0.0005	0.0004	0.0004	0.0004	0.0003	0.0003
$^4S^o_{3/2} - (^3P)\,^2F_{5/2}$	0.0258	0.0256	0.0254	0.0254	0.0254	0.0254	0.0255
$^4S^o_{3/2} - (^1D)\,^2P_{3/2}$	0.0044	0.0041	0.0039	0.0038	0.0037	0.0036	0.0035
$^4S^o_{3/2} - (^1D)\,^2S_{1/2}$	0.0027	0.0025	0.0024	0.0023	0.0022	0.0022	0.0021
$^4S^o_{3/2} - (^3P)\,^2D_{5/2}$	0.0216	0.0219	0.0223	0.0226	0.0230	0.0233	0.0237
$^4S^o_{3/2} - (^3P)\,^2D_{3/2}$	0.0047	0.0044	0.0043	0.0042	0.0041	0.0041	0.0040
$^2D^o_{3/2} - (^3P)\,^4F_{3/2}$	0.0401	0.0390	0.0382	0.0376	0.0372	0.0370	0.0368
$^2D^o_{3/2} - (^3P)\,^4F_{5/2}$	0.0285	0.0258	0.0237	0.0221	0.0208	0.0197	0.0188
$^2D^o_{3/2} - (^1D)\,^2F_{5/2}$	0.0179	0.0169	0.0162	0.0156	0.0152	0.0149	0.0146
$^2D^o_{3/2} - (^3P)\,^4D_{1/2}$	0.0284	0.0291	0.0297	0.0303	0.0308	0.0313	0.0318
$^2D^o_{3/2} - (^3P)\,^4D_{3/2}$	0.0086	0.0076	0.0068	0.0062	0.0057	0.0053	0.0049
$^2D^o_{3/2} - (^3P)\,^4D_{5/2}$	0.0370	0.0360	0.0353	0.0348	0.0345	0.0342	0.0340
$^2D^o_{3/2} - (^3P)\,^2P_{3/2}$	1.5030	1.5750	1.6370	1.6920	1.7410	1.7850	1.8260
$^2D^o_{3/2} - (^3P)\,^4P_{5/2}$	0.0461	0.0466	0.0472	0.0477	0.0484	0.0490	0.0496
$^2D^o_{3/2} - (^3P)\,^2P_{1/2}$	1.6650	1.7440	1.8130	1.8740	1.9280	1.9760	2.0210
$^2D^o_{3/2} - (^3P)\,^4P_{3/2}$	0.0202	0.0204	0.0207	0.0209	0.0212	0.0214	0.0217
$^2D^o_{3/2} - (^3P)\,^4P_{1/2}$	0.0936	0.0983	0.1024	0.1062	0.1095	0.1126	0.1154
$^2D^o_{3/2} - (^1S)\,^2D_{3/2}$	0.5607	0.5865	0.6089	0.6287	0.6464	0.6625	0.6772
$^2D^o_{3/2} - (^1S)\,^2D_{5/2}$	0.0773	0.0806	0.0835	0.0861	0.0884	0.0906	0.0925
$^2D^o_{3/2} - (^1D)\,^2D_{3/2}$	3.2800	3.4400	3.5780	3.7000	3.8100	3.9090	4.0000
$^2D^o_{3/2} - (^1D)\,^2D_{5/2}$	0.1815	0.1896	0.1967	0.2029	0.2086	0.2137	0.2184
$^2D^o_{3/2} - (^1D)\,^2P_{1/2}$	0.2285	0.2389	0.2479	0.2559	0.2631	0.2697	0.2757
$^2D^o_{3/2} - (^3P)\,^2F_{5/2}$	7.2120	7.5740	7.8870	8.1640	8.4130	8.6380	8.8440
$^2D^o_{3/2} - (^1D)\,^2P_{3/2}$	0.0818	0.0845	0.0870	0.0892	0.0912	0.0930	0.0946
$^2D^o_{3/2} - (^1D)\,^2S_{1/2}$	0.0649	0.0678	0.0703	0.0726	0.0747	0.0766	0.0783
$^2D^o_{3/2} - (^3P)\,^2D_{5/2}$	0.0137	0.0134	0.0133	0.0131	0.0131	0.0130	0.0129
$^2D^o_{3/2} - (^3P)\,^2D_{3/2}$	0.0184	0.0184	0.0185	0.0186	0.0188	0.0189	0.0190
$^2D^o_{5/2} - (^3P)\,^4F_{3/2}$	0.0028	0.0024	0.0022	0.0020	0.0019	0.0018	0.0017
$^2D^o_{5/2} - (^3P)\,^4F_{5/2}$	0.0180	0.0174	0.0170	0.0167	0.0165	0.0164	0.0163
$^2D^o_{5/2} - (^3P)\,^4F_{7/2}$	0.0292	0.0267	0.0249	0.0234	0.0223	0.0213	0.0206
$^2D^o_{5/2} - (^1D)\,^2F_{5/2}$	0.0367	0.0355	0.0347	0.0342	0.0338	0.0335	0.0333
$^2D^o_{5/2} - (^3P)\,^4D_{7/2}$	0.0675	0.0646	0.0626	0.0610	0.0598	0.0589	0.0581
$^2D^o_{5/2} - (^3P)\,^4D_{3/2}$	0.0476	0.0486	0.0496	0.0505	0.0514	0.0522	0.0530
$^2D^o_{5/2} - (^3P)\,^4D_{5/2}$	0.0475	0.0443	0.0419	0.0400	0.0385	0.0373	0.0363

Table 9. continued

Transition	T_e (10^6 K)						
($3s^2\,3p^3 \rightarrow 3s^2\,3p^2\,3d$)	4	5	6	7	8	9	10
$^2D^o_{5/2} - (^1D)\,^2F_{7/2}$	0.0536	0.0512	0.0496	0.0484	0.0475	0.0467	0.0461
$^2D^o_{5/2} - (^1D)\,^2G_{7/2}$	0.0656	0.0649	0.0646	0.0645	0.0646	0.0647	0.0650
$^2D^o_{5/2} - (^3P)\,^2P_{3/2}$	3.8780	4.0570	4.2130	4.3510	4.4740	4.5860	4.6880
$^2D^o_{5/2} - (^3P)\,^4P_{5/2}$	0.1435	0.1489	0.1538	0.1581	0.1621	0.1657	0.1691
$^2D^o_{5/2} - (^3P)\,^4P_{3/2}$	0.0340	0.0341	0.0344	0.0347	0.0350	0.0354	0.0357
$^2D^o_{5/2} - (^1S)\,^2D_{3/2}$	0.3942	0.4127	0.4288	0.4430	0.4558	0.4674	0.4781
$^2D^o_{5/2} - (^1S)\,^2D_{5/2}$	2.6310	2.7600	2.8730	2.9710	3.0600	3.1400	3.2130
$^2D^o_{5/2} - (^1D)\,^2D_{3/2}$	0.5765	0.6028	0.6258	0.6462	0.6645	0.6812	0.6965
$^2D^o_{5/2} - (^1D)\,^2D_{5/2}$	3.8380	4.0240	4.1860	4.3290	4.4570	4.5730	4.6790
$^2D^o_{5/2} - (^3P)\,^2F_{5/2}$	0.4458	0.4644	0.4808	0.4955	0.5088	0.5210	0.5322
$^2D^o_{5/2} - (^1D)\,^2P_{3/2}$	0.0547	0.0561	0.0573	0.0585	0.0595	0.0605	0.0614
$^2D^o_{5/2} - (^3P)\,^2F_{7/2}$	10.250	10.750	11.200	11.590	11.940	12.260	12.550
$^2D^o_{5/2} - (^3P)\,^2D_{5/2}$	0.3112	0.3228	0.3334	0.3430	0.3518	0.3599	0.3673
$^2D^o_{5/2} - (^3P)\,^2D_{3/2}$	0.0285	0.0283	0.0283	0.0284	0.0285	0.0286	0.0287
$^2P^o_{1/2} - (^3P)\,^4F_{3/2}$	0.0069	0.0066	0.0063	0.0061	0.0060	0.0059	0.0058
$^2P^o_{1/2} - (^3P)\,^4D_{1/2}$	0.0076	0.0072	0.0069	0.0067	0.0065	0.0063	0.0062
$^2P^o_{1/2} - (^3P)\,^4D_{3/2}$	0.0088	0.0079	0.0073	0.0068	0.0064	0.0060	0.0058
$^2P^o_{1/2} - (^3P)\,^2P_{3/2}$	0.1623	0.1687	0.1744	0.1794	0.1840	0.1881	0.1919
$^2P^o_{1/2} - (^3P)\,^2P_{1/2}$	0.4133	0.4321	0.4482	0.4624	0.4750	0.4865	0.4969
$^2P^o_{1/2} - (^3P)\,^4P_{3/2}$	0.0024	0.0021	0.0019	0.0017	0.0016	0.0015	0.0014
$^2P^o_{1/2} - (^3P)\,^4P_{1/2}$	0.0157	0.0163	0.0168	0.0173	0.0177	0.0181	0.0185
$^2P^o_{1/2} - (^1S)\,^2D_{3/2}$	0.0088	0.0079	0.0072	0.0067	0.0063	0.0060	0.0057
$^2P^o_{1/2} - (^1D)\,^2D_{3/2}$	0.4420	0.4632	0.4816	0.4977	0.5121	0.5252	0.5371
$^2P^o_{1/2} - (^1D)\,^2P_{1/2}$	0.0054	0.0057	0.0060	0.0063	0.0066	0.0069	0.0071
$^2P^o_{1/2} - (^1D)\,^2P_{3/2}$	1.1000	1.1550	1.2010	1.2420	1.2790	1.3120	1.3430
$^2P^o_{1/2} - (^1D)\,^2S_{1/2}$	2.0290	2.1290	2.2160	2.2920	2.3600	2.4220	2.4790
$^2P^o_{1/2} - (^3P)\,^2D_{3/2}$	3.5050	3.6790	3.8310	3.9660	4.0860	4.1950	4.2940
$^2P^o_{3/2} - (^3P)\,^4F_{3/2}$	0.0029	0.0025	0.0023	0.0020	0.0019	0.0017	0.0016
$^2P^o_{3/2} - (^3P)\,^4F_{5/2}$	0.0071	0.0066	0.0062	0.0060	0.0058	0.0057	0.0055
$^2P^o_{3/2} - (^1D)\,^2F_{5/2}$	0.0196	0.0174	0.0157	0.0144	0.0134	0.0125	0.0118
$^2P^o_{3/2} - (^3P)\,^4D_{1/2}$	0.0163	0.0166	0.0168	0.0170	0.0172	0.0174	0.0176
$^2P^o_{3/2} - (^3P)\,^4D_{3/2}$	0.0132	0.0123	0.0117	0.0112	0.0109	0.0106	0.0103
$^2P^o_{3/2} - (^3P)\,^4D_{5/2}$	0.0066	0.0059	0.0054	0.0050	0.0047	0.0045	0.0043
$^2P^o_{3/2} - (^3P)\,^2P_{3/2}$	0.4966	0.5172	0.5350	0.5508	0.5649	0.5778	0.5895
$^2P^o_{3/2} - (^3P)\,^4P_{5/2}$	0.0088	0.0077	0.0069	0.0064	0.0059	0.0055	0.0052
$^2P^o_{3/2} - (^3P)\,^2P_{1/2}$	0.7750	0.8094	0.8392	0.8655	0.8891	0.9105	0.9300
$^2P^o_{3/2} - (^3P)\,^4P_{3/2}$	0.0188	0.0186	0.0186	0.0187	0.0188	0.0189	0.0191
$^2P^o_{3/2} - (^3P)\,^4P_{1/2}$	0.0175	0.0181	0.0187	0.0193	0.0198	0.0203	0.0207
$^2P^o_{3/2} - (^1S)\,^2D_{3/2}$	0.0612	0.0620	0.0629	0.0637	0.0645	0.0652	0.0659
$^2P^o_{3/2} - (^1S)\,^2D_{5/2}$	0.3064	0.3180	0.3283	0.3374	0.3456	0.3531	0.3599
$^2P^o_{3/2} - (^1D)\,^2D_{3/2}$	0.0283	0.0286	0.0289	0.0293	0.0297	0.0301	0.0305
$^2P^o_{3/2} - (^1D)\,^2D_{5/2}$	0.5658	0.5896	0.6105	0.6292	0.6460	0.6613	0.6754
$^2P^o_{3/2} - (^1D)\,^2P_{1/2}$	1.8760	1.9660	2.0430	2.1120	2.1740	2.2290	2.2800
$^2P^o_{3/2} - (^3P)\,^2F_{5/2}$	0.0357	0.0343	0.0334	0.0329	0.0326	0.0324	0.0323
$^2P^o_{3/2} - (^1D)\,^2P_{3/2}$	3.2130	3.3680	3.5030	3.6220	3.7280	3.8250	3.9130
$^2P^o_{3/2} - (^1D)\,^2S_{1/2}$	0.0127	0.0131	0.0135	0.0139	0.0143	0.0146	0.0150
$^2P^o_{3/2} - (^3P)\,^2D_{5/2}$	7.0440	7.3910	7.6930	7.9600	8.1990	8.4160	8.6140
$^2P^o_{3/2} - (^3P)\,^2D_{3/2}$	1.1210	1.1750	1.2230	1.2640	1.3020	1.3360	1.3670

for the stronger $^2P^o_{3/2} - (^1D)\,^2P_{1/2}$ transition, against a difference of more than a factor of 2 shown in Table 5. In F77 it is clearly stated that, due to the neglect of excited configurations of the $1^2\,2^8\,3^5$ even parity complex, the wavefunctions of some of the $3s^2\,3p^2\,3d$ excited states might be substantially wrong in that work. The strong mixing of the levels mentioned above depends critically on the target basis expansion and we propose that the mislabelling affecting the F77 data might be due to his use of an incomplete target basis set.

One last point of discussion concerns the assignment of observed energy values in F77. In that work experimental energies are derived from transition wavelengths given in Fawcett (1971), who provided data for the $(^1D)\,^2D$ term but not for the $(^1S)\,^2D$ term. In our calculation (see Table 1) the $(^1S)\,^2D_J$ levels are energetically lower than the $(^1D)\,^2D_J$ levels but F77 seems to suggest a reversed ordering in his listing, despite the lack of any clear indication of term parentages. A SUPERSTRUCTURE calculation with only 4 configurations in the basis set, performed to mimic the F77 atomic model, revealed that the $(^1D)\,^2D_J$ levels are indeed still energetically higher than the $(^1S)\,^2D_J$ levels, providing a clue to a possible misassignment in F77. By reassigning the 553855 cm^{-1} and 554575 cm^{-1} observed energies to the second lowest $3s^2\,3p^2\,3d\,^2D$ doublet in his Table 1 we would get proper agreement with our results and with the updated observed energies by Corliss & Sugar (1982).

4. Discussion and conclusions

New electron collisional data for $3s^2\,3p^3 - 3s\,3p^4$ and $3s^2\,3p^3 - 3s^2\,3p^2\,3d$ electric dipole transitions in Fe XII have been presented in this paper and compared with previous available computations.

A comparison with the calculations by F77 and TH88 is possible for the $3s^2\,3p^3 - 3s\,3p^4$ transitions. Despite the use of the same *R-matrix* approach for the scattering problem in TH88 and in the present work, we get marginally better agreement with the data obtained by F77 in a *distorted wave* approximation. This is probably due to the inclusion of orbitals of correlation type in the target wavefunctions adopted by TH88. It is pointed out that the most serious discrepancies between the different data sets occur at small collision strength values, where cancellation effects due to the particular choice of target representation are likely to play a bigger role. This shows the importance of using a comprehensive target expansion in the electron scattering computation.

The only set of $3s^2\,3p^3 - 3s^2\,3p^2\,3d$ electric dipole collisional data previously published is that of F77. As stressed in Sect. 3 our results benefit from a greatly improved target representation, a more sophisticated scattering technique, proper inclusion of resonance effects and provision of data over a wide range of electron energies and temperatures. A careful comparison between the two data sets has made possible the identification of some problems in the F77 data, such as mislabellings and observed energies misassignments. These are thoroughly discussed in Sect. 3.2.

In summary, the data presented in this paper represent a significant improvement over previous computations. These data, together with those reported in BMS, should provide a valuable tool for future astrophysical and plasma diagnostic work involving the Fe XII ion.

Acknowledgements. This research was supported by PPARC grants GR/H94979 and GR/K98506 for the IRON Project meetings and CRAY computing time.

References

Arnauld M., Rajmond J., 1992, ApJ 398, 394
Berrington K.A., Eissner W.B., Norrington P.H., 1995, Computer Phys. Commun. 92, 290
Binello A.M., Mason H.E., Storey P.J., 1998, A&AS, 127
Bromage G.E., Cowan R.D., Fawcett B.C., 1978, MNRAS 183, 19
Burgess A., Tully J.A., 1978, J. Phys. B: Atom. Molec. Phys. 11, 4271
Burgess A., Tully J.A., 1992, A&A 254, 436
Burgess A., Hummer D.G., Tully J.A., 1970, Phil. Trans. R. Soc. London, Ser. A 266, 225
Corliss C., Sugar J., 1982, J. Phys. Chem. Ref. Data 11, 135
Eissner W., Jones M., Nussbaumer H., 1974, Computer Phys. Commun. 8, 270
Fawcett B.C., 1971, J. Phys. B: Atom. Molec. Phys. 4, 1577
Fawcett B.C., 1986, ADNDT 35, 203
Feldman U., Cohen L., Doschek G.A., 1983, ApJ 273, 822
Flower D.R., 1977, A&A 54, 163
Hummer D.G., Berrington K.A., Eissner W., Pradhan A.K., Saraph H.E., Tully J.A., 1993, A&A 279, 298
Jupen C., Isler R.C., Träbert E., 1993, MNRAS 264, 627
Kastner S.O., Mason H.E., 1978, A&A 67, 119
Mason H.E., Young P.R., Pike C.D., Harrison R.A., Fludra A., Bromage B.J.I., Del Zanna G., 1997, Solar Phys. 170, 143
Nussbaumer H., Storey P.J., 1978, A&A 64, 139
Tayal S.S., Henry R.J.W., 1986, ApJ 302, 200
Tayal S.S., Henry R.J.W., 1988, ApJ 329, 1023
Tayal S.S., Henry R.J.W., Pradhan A.K., 1987, ApJ 319, 951
van Regemorter H., 1960, MNRAS 121, 213
Withbroe G.L., Raymond J.C., 1984, ApJ 285, 347